

# Transport and entanglement growth in long-range random Clifford circuits

Jonas Richter,<sup>1,2,3</sup> Oliver Lunt,<sup>4,5</sup> and Arijeet Pal<sup>1</sup>

<sup>1</sup>*Department of Physics and Astronomy, University College London, Gower Street, London, WC1E 6BT, UK*

<sup>2</sup>*Department of Physics, Stanford University, Stanford, CA 94305, USA*

<sup>3</sup>*Institut für Theoretische Physik, Leibniz Universität Hannover, Appelstraße 2, 30167 Hannover, Germany*

<sup>4</sup>*Department of Physics, King's College London, Strand, London, WC2R 2LS, UK*

<sup>5</sup>*School of Physics and Astronomy, University of Birmingham, Birmingham, B15 2TT, UK*

(Dated: March 6, 2023)

Conservation laws can constrain entanglement dynamics in isolated quantum systems, manifest in a slowdown of higher Rényi entropies. Here, we explore this phenomenon in a class of long-range random Clifford circuits with U(1) symmetry where transport can be tuned from diffusive to superdiffusive. We unveil that the different hydrodynamic regimes reflect themselves in the asymptotic entanglement growth according to  $S(t) \propto t^{1/z}$ , where the dynamical transport exponent  $z$  depends on the probability  $\propto r^{-\alpha}$  of gates spanning a distance  $r$ . For sufficiently small  $\alpha$ , we show that the presence of hydrodynamic modes becomes irrelevant such that  $S(t)$  behaves similarly in circuits with and without conservation law. We explain our findings in terms of the inhibited operator spreading in U(1)-symmetric Clifford circuits, where the emerging light cones can be understood in the context of classical Lévy flights. Our work sheds light on the connections between Clifford circuits and more generic many-body quantum dynamics.

**Introduction.**— Fundamental questions on the origin of quantum statistical mechanics have experienced a renaissance in recent years [1–3], with experiments being able to probe chaos and information scrambling [4–7]. While much progress has been made due to sophisticated numerical methods (e.g., [8–13]), ideas from quantum information provide a useful lens on quantum dynamics far from equilibrium. In particular, suitable random-circuit models capture aspects of generic quantum systems [14–17], including settings with conservation laws and constraints [18–20], as well as dual-unitary [21, 22], time-periodic [23, 24], or nonunitary dynamics [25, 26]. Random circuits are particularly attractive in view of today’s noisy intermediate-scale quantum devices [27–29], with applications in achieving a quantum computational advantage [30] and exploring operator entanglement [31].

In case of chaotic quantum systems with short-ranged interactions, conservation laws give rise to hydrodynamic modes that typically decay diffusively [32–35], while entanglement is expected to grow ballistically [36]. Remarkably, recent work unveiled that this picture is incomplete and that transport and entanglement are intimately connected [37–41]. Specifically, diffusive transport can constrain higher Rényi entropies to increase diffusively [37],

$$S_{n>1}(t) \propto \sqrt{t}, \quad \text{where } S_n = \log_2 \text{tr}[\rho_A^n]/(1-n), \quad (1)$$

with  $\rho_A = \text{tr}_B |\psi(t)\rangle \langle \psi(t)|$  denoting the reduced density matrix for a bipartition into subsystems  $A$  and  $B$ , and  $|\psi(t)\rangle$  is the state of the system. In contrast, the von Neumann entropy  $S_1 = -\text{tr}[\rho_A \log_2 \rho_A]$  grows linearly as usual,  $S_1(t) \propto t$ . In this Letter, we demonstrate that constrained entanglement dynamics occurs more generically also for other transport types, and can be readily explored in U(1)-symmetric long-range Clifford circuits [Fig. 1 (a)]. Depending on the probability  $\propto r^{-\alpha}$  of gates

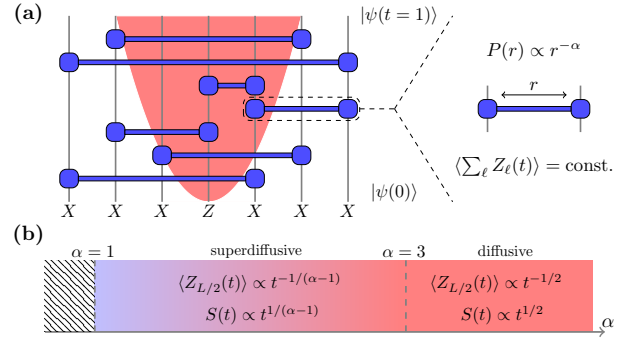


FIG. 1. (a) Two-qubit Clifford gates of range  $r$  occur with probability  $P(r) \propto r^{-\alpha}$  and conserve the total Pauli-Z component [92]. (b) By tuning  $\alpha > 1$ , different hydrodynamic regimes with dynamical exponent  $z$  [Eq. (2)] emerge, manifest in the tails of the circuit-averaged expectation value  $\langle Z_{L/2}(t) \rangle \propto t^{-1/z}$ . Entanglement saturates approximately on a time scale  $\propto L^z$ , implying that it asymptotically mirrors the transport behavior,  $S(t) \propto t^{1/z}$ .

spanning a distance  $r$ , the emerging transport can be tuned from diffusive to superdiffusive. These circuits can be seen as minimal models to describe the scrambling dynamics of long-range Hamiltonian systems. Specifically, it was found in [42, 43] that the light-cone spreading in such circuits is very similar to the dynamics generated by Hamiltonians with interactions decaying as  $\propto r^{-\alpha'}$ , where  $\alpha' = \alpha/2$ . While Clifford gates are insufficient for universal quantum computation, they form unitary 2-designs [44] (3-designs for qubits [45]), such that circuit averages of certain quantities, e.g., out-of-time-ordered correlators, coincide with Haar averages over the full unitary group [15, 16]. Clifford circuits can thus be useful to study aspects of more generic quantum dynamics.

Long-range interactions are ubiquitous in nature, in-

cluding dipolar or van der Waals interactions [46], experimentally realized in various platforms [47–53]. In contrast to short-range models, where Lieb-Robinson bounds confine correlations to a linear “light cone” [54], long-range interactions may lead to faster information propagation [55, 56]. Much effort has been invested to tighten Lieb-Robinson-like bounds for power-law interacting models [42, 57–67], and to study transport and entanglement dynamics [43, 68–77]. For chaotic systems in  $d$  dimensions, it was argued that linear light cones arise for  $\alpha' > d + 1/2$  with properties similar to short-range models, while power-law or logarithmic bounds emerge for  $d/2 < \alpha' < d + 1/2$  [42, 64]. For  $\alpha' < d/2$ , locality breaks down and information propagation becomes essentially instantaneous [78].

From a numerical point of view, long-range systems are challenging due to quick entanglement generation and strong finite-size effects [79]. In contrast, the random Clifford circuits considered here can be simulated efficiently even for large systems. Summarizing our main results, we unveil a direct correspondence between transport and entanglement, with entanglement saturating on a time scale  $t_{\text{sat}} \propto L^z$  implying an asymptotic scaling  $S(t) \propto t^{1/z}$ , where  $z$  is the dynamical transport exponent [Fig. 1 (b)]. We explain this finding in terms of the inhibited operator spreading in U(1)-symmetric Clifford circuits, leading to narrower light cones compared to circuits without conservation law. Moreover, we demonstrate that the constraint on  $S(t)$  becomes insignificant once the dynamical exponent for transport reaches  $z \approx 1$ .

*Clifford circuits with symmetry.*— Clifford circuits are of major interest in quantum information [80], including error correction and randomized benchmarking [81, 82]. In the context of quantum dynamics, they recently gained popularity to study measurement-induced entanglement transitions (e.g., [43, 83–87]) as their efficient simulability allows to access large system sizes [88, 89]. The key idea is to exploit the stabilizer formalism [80, 90], where a state  $|\psi\rangle$  on  $L$  qubits can be uniquely defined by  $L$  operators  $\mathcal{O}_i$ , i.e.,  $\mathcal{O}_i |\psi\rangle = |\psi\rangle$ , where  $\mathcal{O}_i = X_1^{\nu_1^i} Z_1^{\mu_1^i} \dots X_\ell^{\nu_\ell^i} Z_\ell^{\mu_\ell^i} \dots X_L^{\nu_L^i} Z_L^{\mu_L^i}$  are  $L$ -site Pauli strings and  $\nu_\ell^i, \mu_\ell^i = \{0, 1\}$  [88]. Since Clifford gates preserve the Pauli group, the action  $|\psi\rangle \rightarrow \mathcal{U} |\psi\rangle$  of a Clifford gate  $\mathcal{U}$  can be efficiently described by the stabilizers,  $\mathcal{U} \mathcal{O}_i \mathcal{U}^\dagger$  [91], e.g., by storing the  $\nu_\ell^i, \mu_\ell^i$  in a binary matrix  $\mathcal{M}$  and updating their values appropriately [88].

We show that random Clifford circuits can elucidate the interplay between transport and entanglement [39]. We consider circuits with U(1) symmetry, where one time step is defined as the application of  $L$  gates conserving the total magnetization,  $\langle \psi(t) | \sum_\ell Z_\ell | \psi(t) \rangle = \text{const.}$  [Fig. 1]. This property is quite restrictive: While the full two-qubit Clifford group has 11520 distinct elements (modulo a global phase), only 64 conserve the total Pauli-Z component, see [92]. Due to the U(1) symmetry and the Pauli-preserving property of Clifford gates, it turns out that transport can

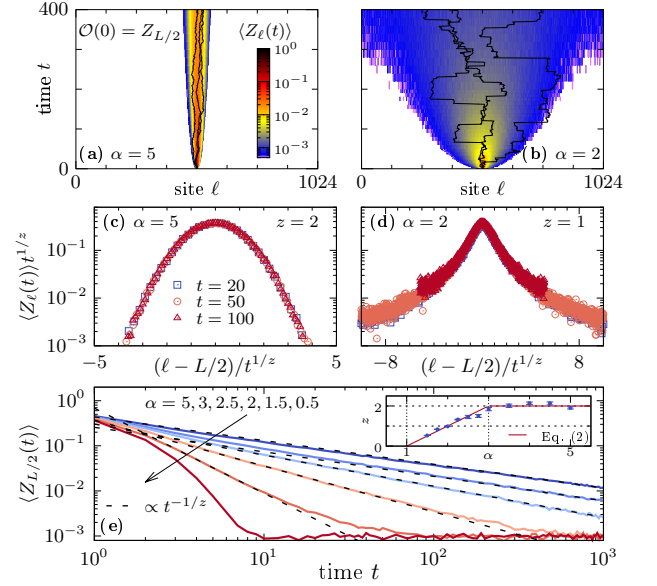


FIG. 2. [(a),(b)]  $\langle Z_\ell(t) \rangle$  averaged over  $\sim 10^5$  circuit realizations for  $\alpha = 5$  and  $\alpha = 2$  and  $L = 1024$ . Solid curves indicate individual realizations, i.e., random-walks with step-size distribution  $\propto r^{-\alpha}$ . [(c),(d)]  $\langle Z_\ell(t) \rangle t^{1/z}$  at fixed  $t$ , plotted against  $(\ell - L/2)/t^{1/z}$ . (e)  $\langle Z_{L/2}(t) \rangle$  for different  $\alpha$ . Dashed lines indicate power law  $\propto t^{-1/z}$ . Inset shows  $z$  extracted from the fits and compared to Eq. (2).

be understood classically in terms of long-range random walks, so called Lévy flights [53, 69, 95, 96]. However, we will show that such constrained circuits still generate extensive entanglement, similar to Haar-random circuits [14].

Product states such as  $|\rightarrow\rangle^{\otimes L}$  with spins in the  $x$  direction can be stabilized by operators  $\mathcal{O}_i = X_i$  ( $i = 1, \dots, L$ ) acting nontrivially only on a single site. Evolving  $|\psi\rangle$  with respect to a random circuit will cause the  $\mathcal{O}_i$  to become nonlocal, resulting in increased entanglement. Clifford circuits are special as they generate flat entanglement spectra such that all  $S_n$  are equivalent [97]. While the different behaviors of  $S_1$  and  $S_{n>1}$  demonstrated in [37] therefore cannot be resolved,  $S(t)$  is nevertheless sensitive to conservation laws and  $S(t) \propto \sqrt{t}$  was found in Clifford circuits with diffusive transport [39]. Here, we show that long-range circuits provide an ideal framework to study entanglement dynamics also for other transport types. To this end, we reiterate the arguments to explain the constrained entanglement growth [37, 38]: Consider the reduced density matrix  $\rho_A$  with  $\chi$  nonzero eigenvalues  $\Lambda_1 \leq \dots \leq \Lambda_\chi$ . In the presence of hydrodynamic modes with dynamical exponent  $z$ ,  $\Lambda_\chi$  can be bounded by  $\Lambda_\chi \gtrsim e^{-\gamma t^{1/z}}$  with some constant  $\gamma$ , where  $z = 2$  corresponds to diffusion [37, 38]. The bound results from rare contributions to  $|\psi(t)\rangle$ , where a region of length  $\xi$  around the cut between  $A$  and  $B$  is in the  $|\uparrow\rangle$  state, acting as a bottleneck for entanglement as it takes time

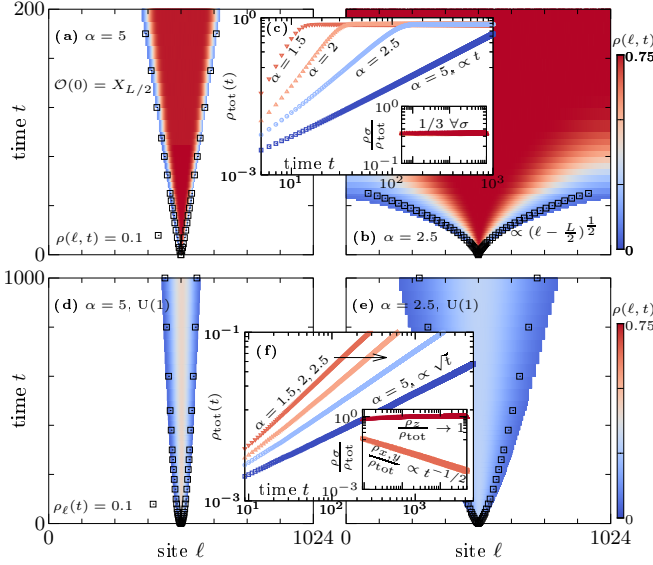


FIG. 3. [(a),(b)] Averaged  $\rho(\ell, t)$  in full Clifford circuits with  $\alpha = 5$  and  $\alpha = 2.5$ , obtained from  $\mathcal{O}(0) = X_{L/2}$  with  $L = 1024$ . Symbols indicate  $\rho(\ell, t) = 10^{-1}$ . (c)  $\rho_{\text{tot}}(t)$  for  $L = 2048$  and different  $\alpha$  (see also [92]). Inset shows  $\rho_{\sigma}(t)/\rho_{\text{tot}}(t) \approx 1/3$ , i.e., all  $\Sigma^{\sigma}$  contribute equally. [(d),(e),(f)] Analogous data, but for U(1)-symmetric circuits, where  $\mathcal{O}(t)$  spreads significantly slower. This stems from the dominant contribution of  $Z$  operators within  $\rho_{\text{tot}}(t)$ , cf. inset in (f) for  $\alpha = 5$ .

$\propto \xi^z$  for a  $|\downarrow\rangle$  to get across the cut. It follows that  $S_{n \rightarrow \infty} = -\log_2 \Lambda_{\chi}$  scales as  $S_{\infty}(t) \propto t^{1/z}$  and, due to  $S_{\infty} \leq S_{n>1} \leq n S_{\infty}/(n-1)$ , all  $S_{n>1}(t)$  obey this scaling. This is independent of the type of time evolution and generalizes to Clifford circuits, where  $\Lambda_i = \Lambda$  and  $S_n(t) \equiv S(t)$ .

*Hydrodynamics.*— By varying  $\alpha$ , it is possible to tune the nature of transport. Consider a state  $|\psi\rangle = |\rightarrow\rangle^{\otimes L/2-1} |\uparrow\rangle |\rightarrow\rangle^{\otimes L/2}$ , stabilized by  $X_{\ell}$  for  $\ell \neq L/2$ , and  $Z_{\ell}$  for  $\ell = L/2$ , cf. Fig. 1 (a). The action  $\mathcal{U}\mathcal{O}_i\mathcal{U}^{\dagger}$  of U(1)-symmetric Clifford gates on the two classes of stabilizers is quite different. While the  $X_{\ell}$  becomes nonlocal and generates entanglement, the stabilizer  $Z_{L/2}$  remains of length one throughout the circuit [92]. Specifically, the  $Z$  operator performs  $\alpha$ -dependent random walks, i.e., Lévy flights [53, 69], examples of which are shown in Figs. 2 (a), (b) for  $\alpha = 5$  and  $\alpha = 2$ . Consequently, at a given time, there will be a site  $\ell$  with  $\langle\psi(t)|Z_{\ell}|\psi(t)\rangle = 1$  unentangled with the rest of the system [98].

Simulating 1d circuits with  $L = 1024$ , Figs. 2 (a), (b) show the circuit-averaged value  $\langle Z_{\ell}(t) \rangle$  for  $\sim 10^5$  random realizations of  $\mathcal{U}Z_{L/2}\mathcal{U}^{\dagger}$ , highlighting a change from local to non-local when reducing  $\alpha$ . Analyzing  $\langle Z_{\ell}(t) \rangle$  at fixed  $t$ , we find Gaussian profiles for  $\alpha = 5$  that collapse when rescaled appropriately [Fig. 2 (c)], indicating diffusion. In contrast,  $\langle Z_{\ell}(t) \rangle$  is non-Gaussian for  $\alpha = 2$  but rather described by a Lorentzian, signaling superdiffusive transport [68, 69]. (See [92] for other  $\alpha$  and 2d circuits.) The

$\alpha$ -dependent transport regimes are also reflected in the decay at  $\ell = L/2$ ,  $\langle Z_{L/2}(t) \rangle \propto t^{-1/z}$ , where  $z$  approximately follows the Lévy-flight prediction [53, 69, 99],

$$z = \begin{cases} 2, & \alpha \geq 3; \\ \alpha - 1, & 1 < \alpha < 3, \end{cases} \quad (2)$$

with no hydrodynamic tail for  $\alpha \leq 1$  [Fig. 2 (e)]. Clifford and U(1)-symmetric Haar-random gates are expected to yield the same circuit-averaged  $\langle Z_{\ell}(t) \rangle$ . In contrast, individual circuit realizations differ since Haar gates distribute the  $Z$  excitation smoothly over multiple sites whereas Clifford gates yield sharp random walks. The transport behavior in Fig. 2 agrees qualitatively with the emergent quantum hydrodynamics observed in long-range Hamiltonian systems [53, 69]. Even though transport in the Clifford case is a purely classical process, the average coarse-grained type of hydrodynamics, both in the circuit and the Hamiltonian model, is especially at high temperatures mainly set by the range of the interactions (i.e., by  $\alpha$ ), and not so much by the microscopic dynamics.

*Operator spreading.*— While  $\mathcal{U}Z_{\ell}\mathcal{U}^{\dagger}$  remains a single-site operator for U(1)-symmetric Clifford gates [Fig. 2], we now consider  $\mathcal{O} = X_{\ell}$ . Generally,  $\mathcal{O}(t) = \sum_{\mathcal{S}} \alpha_{\mathcal{S}}(t) \mathcal{S}$  can be written in the basis of the  $4^L$  Pauli strings  $\mathcal{S}$ . Evolution under Haar-random gates increases the number of nonzero  $\alpha_{\mathcal{S}}(t)$  [14–16], leading to operator entanglement [100]. In contrast, Clifford gates map Pauli operators to each other,  $\mathcal{O}(t) = \delta_{\mathcal{S}, \mathcal{O}(t)} \mathcal{S}$ , with no operator entanglement. However,  $\mathcal{O}(t)$  will become nonlocal, manifested by its growing support  $\rho_{\text{tot}}(t) = \frac{1}{L} \sum_{\ell, \sigma} \rho_{\sigma}(\ell, t)$ , where  $\rho_{\sigma}(\ell, t) = \text{tr}[\mathcal{O}_{\ell}(t) \Sigma^{\sigma}]/2$ ,  $\mathcal{O}_{\ell}(t)$  is the matrix at position  $\ell$  in the string, and  $\Sigma^{\sigma} = \{X, Y, Z\}$ ,  $\sigma = x, y, z$ .

Considering  $\mathcal{O}(0) = X_{L/2}$ , we plot  $\rho(\ell, t) = \sum_{\sigma} \rho_{\sigma}(\ell, t)$  in Fig. 3, which is a measure for the out-of-time-ordered correlator between operators at sites  $\ell$  and  $L/2$  [101]. For circuits without conservation law [Figs. 3 (a),(b)], we observe a linear light cone for  $\alpha = 5$ , while a power-law light cone emerges for  $\alpha = 2.5$ , in agreement with the phase diagram in [42]. Correspondingly, we find  $\rho_{\text{tot}}(t) \propto t$  at  $\alpha = 5$  and faster growth for smaller  $\alpha$  [Fig. 3 (c)], see also [92]. In the bulk of the light cone, we observe full scrambling with  $\rho(\ell, t) \rightarrow 3/4$  and  $\rho_{\sigma}(t)/\rho_{\text{tot}}(t) \approx 1/3$  [insets in Fig. 3 (c)], where  $\rho_{\sigma}(t) = \sum_{\ell} \rho_{\sigma}(\ell, t)$  is the Pauli-component resolved support. Speaking differently, the interior of the light cone has reached an equilibrium distribution where local  $X, Y, Z$  operators are equally likely. We will discuss the dynamics of the light-cone edges further below in the context of Fig. 4.

Next, turning to U(1)-symmetric gates, the behavior of  $\rho(\ell, t)$  changes drastically [Figs. 3 (d),(e)]. Namely, operator spreading is significantly slower and resembles the transport behavior of the conserved quantity [Eq. (2)], with a diffusive (superdiffusive) light cone for  $\alpha = 5$  ( $\alpha = 2.5$ ), also reflected in the growth of  $\rho_{\text{tot}}(t)$  [Fig. 3 (f)]. This is due to the properties of the U(1)-symmetric



Clifford gates, which cause  $\mathcal{O}(t)$  to be dominated by  $Z$  operators. Given the initial operator  $\mathcal{O}(0) = X_{L/2}$  with a single  $X$  at  $\ell = L/2$  and identity operators on all other sites, it is in fact significantly more likely that a random gate will generate more  $Z$  than  $X, Y$  operators and thereby increase the overall share of  $Z$  in  $\mathcal{O}(t)$ , see [92] for details. This is shown in the inset of Fig. 3 (f) for  $\alpha = 5$ , where we find  $\rho_z(t) \propto t^{1/2}$  while  $\rho_{x,y}(t) = \text{const.}$  such that  $\rho_z(t)/\rho_{\text{tot}}(t) \rightarrow 1$ . The inhomogeneous composition of  $\mathcal{O}(t)$  differs from the unsymmetric case where  $X, Y, Z$  occur with equal probability [Fig. 3 (c)]. The large fraction of  $Z$  operators behaves similarly to Fig. 2, leading to narrower light cones compared to circuits without conservation law. Furthermore, studying the bulk of the light cone, we find that  $\rho(\ell, t) < 3/4$  in the  $U(1)$ -symmetric case [Fig. 3 (d),(e)]. This indicates that at least on the time scales shown here, the operator string is not fully scrambled and contains on average more identity operators than in the case without conservation law.

The operator spreading in  $U(1)$ -symmetric Clifford circuits is notably simpler compared to the Haar-random case, where the conserved charges lag behind the light-cone front which propagates quickly due to nonconserved operators [18]. While Clifford gates fail to capture this aspect of generic quantum dynamics, the simplified description is helpful to understand the constrained entanglement dynamics since the light cones in Fig. 3 upper bound the growth of  $S(t)$  [14].

*Entanglement dynamics.*— Choosing  $|\psi(0)\rangle = |\rightarrow\rangle^{\otimes L}$ , we study  $S(t) = \text{rank}(\mathcal{M}_{L/2}) - L/2$  for a half-system cut, where  $\mathcal{M}_{L/2}$  denotes the stabilizer matrix of the first  $L/2$  sites [14, 102, 103]. From this expression, it is clear that  $S(t)$  depends on the collective dynamics of  $|\psi(t)\rangle$ 's stabilizers. Since  $|\psi(0)\rangle$  is a superposition of all symmetry sectors,  $S(t \rightarrow \infty) \approx L/2$  saturates at the same value in circuits with and without the conservation law [Figs. 4 (a),(b)]. We find it convenient to analyze the  $\alpha$ -dependence of  $S(t)$  by extracting the saturation time  $t_{\text{sat}} \propto L^z$  for different  $L$ , implying an asymptotic scaling  $S(t) \propto t^{1/z}$ . The obtained values of  $z$  are summarized in Fig. 4 (e). In the case of  $U(1)$ -symmetric circuits, we find that the transport behavior is reflected in the entanglement dynamics and  $z$  is reasonably well described by Eq. (2). In addition, while we recover  $z \rightarrow 1$  in unsymmetric circuits for  $\alpha \geq 3$ , as expected for short-range models [14], the scaling behaviors of circuits with and without conservation law become similar for  $\alpha \lesssim 2$ , with all discrepancies in  $z$  estimates contained within error bars.

At small  $\alpha$ , transport is fast enough that entanglement growth is mainly dictated by the gate range and not by the conservation law. Specifically, at  $\alpha = 2$  we have  $z \approx 1$  and the bound  $\Lambda_X \gtrsim e^{-\gamma t^{1/z}}$  due to transport becomes comparable to the typical value  $\sim e^{-\gamma t}$  expected given the ballistic  $S_1(t)$  in generic circuits [37]. The behavior of the

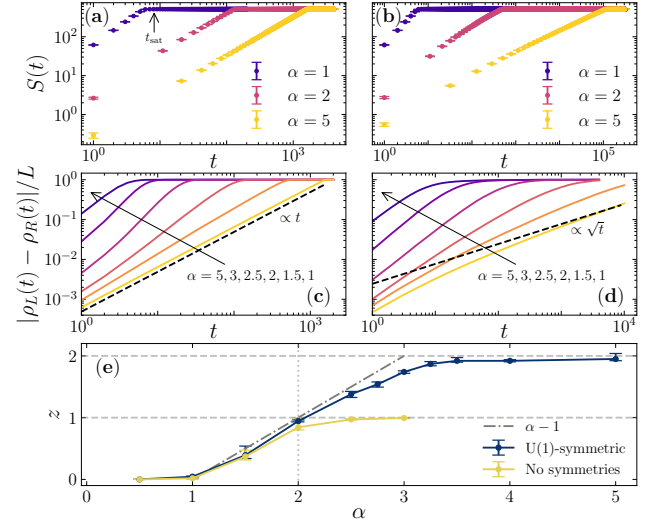


FIG. 4. [(a),(b)]  $S(t)$  for different  $\alpha$  in asymmetric and  $U(1)$ -symmetric circuits with  $L = 1024$  and open boundaries. For  $\alpha \geq 3$ , we expect short-range behavior:  $z = 2$  with  $U(1)$  symmetry and  $z = 1$  without. [(c),(d)] Normalized difference between left (right) endpoints of  $\mathcal{O}(t)$  for  $L = 2048$ . The dashed curves indicate  $\propto t$  ( $\propto \sqrt{t}$ ) scaling. (e)  $z$  versus  $\alpha$  for circuits with and without conservation law. The deviations from Eq. (2) around  $\alpha = 3$  may be due to logarithmic corrections to transport [69].

edges of the light cone can provide further quantitative insights. Specifically, we study the endpoints  $\rho_{L(R)}(t)$  of a string  $\mathcal{O}(t)$ , i.e., the left(right)most  $\ell$  where  $\mathcal{O}_\ell(t)$  is nonidentity. Once a nontrivial part of  $\mathcal{O}(t)$  extends across the cut, entanglement may in principle increase. One might therefore expect that  $\rho_{L(R)}(t)$  is more relevant for  $S(t)$  than  $\rho_{\text{tot}}(t)$  [Fig. 3]. As shown in Figs. 4 (c) and (d), we find that  $|\rho_L(t) - \rho_R(t)|/L$  behaves very differently in symmetric and unsymmetric circuits for  $\alpha = 5$ , but grows with roughly comparable rate if  $\alpha$  is small (see also [92]), which is consistent with the observed similar growth rate of entanglement.

We expect the relation between transport and entanglement to carry over to Rényi entropies  $S_{n>1}(t)$  in generic systems with a conserved quantity, see [92] for some evidence in a long-range tilted field Ising model. Since Clifford gates form unitary 3-designs [44, 45], they give the same “annealed” Rényi-2 entropy  $S_2^{(a)} = -\log \text{tr}_A \rho_A^2$  as a Haar-random circuit. Although  $S_2^{(a)} \leq \overline{S}_2$  only lower bounds the average  $\overline{S}_2$ , in  $U(1)$ -symmetric Haar-random circuits it displays the same  $\sqrt{t}$  growth as  $\overline{S}_2$  [37], consistent with small sample-to-sample fluctuations of  $S_2(t)$ .

Let us comment on the deviations in Fig. 4 (e) from the prediction (2), most pronounced near  $\alpha = 3$ . Even for  $L \sim 10^3$  presented here, we observe a drift of  $z$  with  $L$ . We attempt to account for these finite-size effects by restricting the data to  $L \leq L_{\text{end}}$  and extrapolating  $z(L_{\text{end}})$  to  $1/L_{\text{end}} \rightarrow 0$ . For details, including how we obtain the

error bars, see [92]. Precisely at  $\alpha = 3$ , transport can receive logarithmic corrections [69], which may also explain the faster entanglement growth. Repeating our analysis, but with  $S(t) \sim t^{1/z} \sqrt{\log t}$ , we obtain  $z = 1.91(1)$  much closer to  $z = 2$  [104]. The marginality at  $\alpha \approx 3$  is also reflected in the development of non-Gaussian tails in both  $\langle Z_\ell(t) \rangle$  and  $\rho(\ell, t)$  [92].

*Conclusion.*— We have studied the interplay of transport and entanglement dynamics in long-range random Clifford circuits with  $U(1)$  symmetry. We demonstrated that the emerging transport regimes with dynamical exponent  $z$  reflect themselves in the growth of entanglement as  $S(t) \propto t^{1/z}$ , generalizing earlier work that has focused on diffusive systems with  $z = 2$  [37]. While we expect this result to hold also in more generic Haar-random circuits or chaotic quantum systems for  $S_{n>1}(t)$ , we here provided a simplified picture specific to the Clifford framework, where operator strings become dominated by the conserved quantity leading to narrower light cones. While transport in Clifford circuits turned out to be purely classical, their efficient simulability may suggest the study of possible connections with recent state-of-the-art methods to capture transport coefficients [10–12, 105–108], and to better understand the role of entanglement and the differences to full thermalizing quantum dynamics [109].

A promising research direction is to consider entanglement dynamics in Clifford circuits with other gate sets or conservation laws, potentially giving rise to localization [110], as well as adding measurements which can induce nonequilibrium phases in circuits with symmetry [111, 112]. Studying the impact of sporadic non-Clifford gates, acting as seeds of chaos [113], is another natural avenue. Finally, it would be interesting if the transport-dependent entanglement growth is observable in quantum-simulator experiments, where diffusion and superdiffusion can be realized [53, 114] and the Rényi-2 entropy is accessible for small systems [115, 116].

*Acknowledgments.*— We sincerely thank Lluís Masanes for a helpful comment. This work was funded by the European Research Council (ERC) under the European Union’s Horizon 2020 research and innovation programme (Grant agreement No. 853368). J.R. also received funding from the European Union’s Horizon Europe programme under the Marie Skłodowska-Curie grant agreement No. 101060162. O.L. acknowledges support by UK Research and Innovation (UKRI) [grant number MR/T040947/1].

---

[1] L. D’Alessio, Y. Kafri, A. Polkovnikov, and M. Rigol, *From Quantum Chaos and Eigenstate Thermalization to Statistical Mechanics and Thermodynamics*, Adv. Phys. **65**, 239 (2016).  
[2] R. Nandkishore and D. A. Huse, *Many-Body Localization and Thermalization in Quantum Statistical Mechanics*, Annu. Rev. Condens. Matter Phys. **6**, 15 (2015).

[3] B. Bertini, F. Heidrich-Meisner, C. Karrasch, T. Prosen, R. Steinigeweg, and M. Žnidarič, *Finite-temperature transport in one-dimensional quantum lattice models*, Rev. Mod. Phys. **93**, 025003 (2021).  
[4] J. Li, R. Fan, H. Wang, B. Ye, B. Zeng, H. Zhai, X. Peng, and J. Du, *Measuring Out-of-Time-Order Correlators on a Nuclear Magnetic Resonance Quantum Simulator*, Phys. Rev. X **7**, 031011 (2017).  
[5] M. Gärttner, J. G. Bohnet, A. Safavi-Naini, M. L. Wall, J. J. Bollinger, and A. M. Rey, *Measuring out-of-time-order correlations and multiple quantum spectra in a trapped ion quantum magnet*, Nat. Phys. **13**, 781 (2017).  
[6] K. A. Landsman, C. Figgatt, T. Schuster, N. M. Linke, B. Yoshida, N. Y. Yao, and C. Monroe, *Verified quantum information scrambling*, Nature **567**, 61 (2019).  
[7] M. S. Blok, V. V. Ramasesh, T. Schuster, K. O’Brien, J. M. Kreikebaum, D. Dahlen, A. Morvan, B. Yoshida, N. Y. Yao, and I. Siddiqi, *Quantum Information Scrambling on a Superconducting Qutrit Processor*, Phys. Rev. X **11**, 021010 (2021).  
[8] J. Haegeman, J. I. Cirac, T. J. Osborne, I. Pižorn, H. Verschelde, and F. Verstraete, *Time-Dependent Variational Principle for Quantum Lattices*, Phys. Rev. Lett. **107**, 070601 (2011).  
[9] S. Paeckel, T. Köhler, A. Swoboda, S. R. Manmana, U. Schollwöck, and C. Hubig, *Time-evolution methods for matrix-product states*, Ann. Phys. **411**, 167998 (2019).  
[10] T. Rakovszky, C. W. von Keyserlingk, and F. Pollmann, *Dissipation-assisted operator evolution method for capturing hydrodynamic transport*, Phys. Rev. B **105**, 075131 (2022).  
[11] C. D. White, M. Zaletel, R. S. K. Mong, and G. Refael, *Quantum dynamics of thermalizing systems*, Phys. Rev. B **97**, 035127 (2018).  
[12] J. Wurtz, A. Polkovnikov, and D. Sels, *Cluster truncated Wigner approximation in strongly interacting systems*, Ann. Phys. **395**, 341 (2018).  
[13] T. Heitmann, J. Richter, D. Schubert, and R. Steinigeweg, *Selected applications of typicality to real-time dynamics of quantum many-body systems*, Z. Naturforsch. A **75**, 421 (2020).  
[14] A. Nahum, J. Ruhman, S. Vijay, and J. Haah, *Quantum Entanglement Growth under Random Unitary Dynamics*, Phys. Rev. X **7**, 031016 (2017).  
[15] C. W. von Keyserlingk, T. Rakovszky, F. Pollmann, and S. L. Sondhi, *Operator Hydrodynamics, OTOCs, and Entanglement Growth in Systems without Conservation Laws*, Phys. Rev. X **8**, 021013 (2018).  
[16] A. Nahum, S. Vijay, and J. Haah, *Operator Spreading in Random Unitary Circuits*, Phys. Rev. X **8**, 021014 (2018).  
[17] F. G. S. L. Brandão, W. Chemissany, N. Hunter-Jones, R. Kueng, and J. Preskill, *Models of Quantum Complexity Growth*, PRX Quantum **2**, 030316 (2021).  
[18] V. Khemani, A. Vishwanath, and D. A. Huse, *Operator Spreading and the Emergence of Dissipative Hydrodynamics under Unitary Evolution with Conservation Laws*, Phys. Rev. X **8**, 031057 (2018).  
[19] T. Rakovszky, F. Pollmann, and C. W. von Keyserlingk, *Diffusive Hydrodynamics of Out-of-Time-Ordered Correlators with Charge Conservation*, Phys. Rev. X **8**, 031058 (2018).  
[20] S. Moudgalya, A. Prem, D. A. Huse, and A. Chan, *Spectral statistics in constrained many-body quantum chaotic systems*, Phys. Rev. Research **3**, 023176 (2021).

- [21] B. Bertini, P. Kos, and T. Prosen, *Exact Correlation Functions for Dual-Unitary Lattice Models in 1 + 1 Dimensions*, Phys. Rev. Lett. **123**, 210601 (2019).
- [22] P. W. Claeys and A. Lamacraft, *Ergodic and Nonergodic Dual-Unitary Quantum Circuits with Arbitrary Local Hilbert Space Dimension*, Phys. Rev. Lett. **126**, 100603 (2021).
- [23] B. Bertini, P. Kos, and T. Prosen, *Exact Spectral Form Factor in a Minimal Model of Many-Body Quantum Chaos*, Phys. Rev. Lett. **121**, 264101 (2018).
- [24] A. Chan, A. De Luca, and J. T. Chalker, *Spectral Statistics in Spatially Extended Chaotic Quantum Many-Body Systems*, Phys. Rev. Lett. **121**, 060601 (2018).
- [25] B. Skinner, J. Ruhmann, and A. Nahum, *Measurement-Induced Phase Transitions in the Dynamics of Entanglement*, Phys. Rev. X **9**, 031009 (2019).
- [26] A. C. Potter and R. Vasseur, *Entanglement dynamics in hybrid quantum circuits*, arXiv:2111.08018.
- [27] J. Preskill, *Quantum Computing in the NISQ era and beyond*, Quantum **2**, 79 (2018).
- [28] J. Richter and A. Pal, *Simulating Hydrodynamics on Noisy Intermediate-Scale Quantum Devices with Random Circuits*, Phys. Rev. Lett. **126**, 230501 (2021).
- [29] O. Lunt, J. Richter, and A. Pal, *Quantum simulation using noisy unitary circuits and measurements*, arXiv:2112.06682.
- [30] F. Arute et al., *Quantum supremacy using a programmable superconducting processor*, Nature **574**, 505 (2019).
- [31] X. Mi et al., *Information scrambling in quantum circuits*, Science **374**, 1479 (2021).
- [32] J. Lux, J. Müller, A. Mitra, and A. Rosch, *Hydrodynamic long-time tails after a quantum quench*, Phys. Rev. A **89**, 053608 (2014).
- [33] A. Bohrdt, C. B. Mendl, M. Endres, and M. Knap, *Scrambling and thermalization in a diffusive quantum many-body system*, New J. Phys. **19**, 063001 (2017).
- [34] J. Richter, F. Jin, H. De Raedt, K. Michielsen, J. Gemmer, and R. Steinigeweg, *Real-time dynamics of typical and untypical states in nonintegrable systems*, Phys. Rev. B **97**, 174430 (2018).
- [35] J. Richter, F. Jin, L. Knipschild, J. Herbrych, H. De Raedt, K. Michielsen, J. Gemmer, and R. Steinigeweg, *Magnetization and energy dynamics in spin ladders: Evidence of diffusion in time, frequency, position, and momentum*, Phys. Rev. B **99**, 144422 (2019).
- [36] H. Kim and D. A. Huse, *Ballistic Spreading of Entanglement in a Diffusive Nonintegrable System*, Phys. Rev. Lett. **111**, 127205 (2013).
- [37] T. Rakovszky, F. Pollmann, and C. W. von Keyserlingk, *Sub-ballistic Growth of Rényi Entropies due to Diffusion*, Phys. Rev. Lett. **122**, 250602 (2019).
- [38] Y. Huang, *Dynamics of Rényi entanglement entropy in diffusive qudit systems*, IOP SciNotes **1**, 035205 (2020).
- [39] M. Žnidarič, *Entanglement growth in diffusive systems*, Commun. Phys. **3**, 100 (2020).
- [40] T. Rakovszky, F. Pollmann, and C. von Keyserlingk, *Entanglement growth in diffusive systems with large spin*, Commun. Phys. **4**, 91 (2021).
- [41] T. Zhou and A. W. W. Ludwig, *Diffusive scaling of Rényi entanglement entropy*, Phys. Rev. Research **2**, 033020 (2020).
- [42] T. Zhou, S. Xu, X. Chen, A. Guo, and B. Swingle, *Operator Lévy Flight: Light Cones in Chaotic Long-Range Interacting Systems*, Phys. Rev. Lett. **124**, 180601 (2020).
- [43] M. Block, Y. Bao, S. Choi, E. Altman, and N. Y. Yao, *Measurement-Induced Transition in Long-Range Interacting Quantum Circuits*, Phys. Rev. Lett. **128**, 010604 (2022).
- [44] A. W. Harrow and R. A. Low, *Random Quantum Circuits are Approximate 2-designs*, Comm. Math. Phys. **291**, 257 (2009).
- [45] Z. Webb, *The Clifford group forms a unitary 3-design*, Quantum Inf. Comput. **16**, 1379 (2016).
- [46] M. Saffman, T. G. Walker, K. Mølmer, *Quantum information with Rydberg atoms*, Rev. Mod. Phys. **82**, 2313 (2010).
- [47] D. Porras and J. I. Cirac, *Effective Quantum Spin Systems with Trapped Ions*, Phys. Rev. Lett. **92**, 207901 (2004).
- [48] P. Jurcevic, B. P. Lanyon, P. Hauke, C. Hempel, P. Zoller, R. Blatt, and C. F. Roos, *Observation of entanglement propagation in a quantum many-body system*, Nature (London) **511**, 202 (2014).
- [49] J. Smith, A. Lee, P. Richerme, B. Neyenhuis, P. W. Hess, P. Hauke, M. Heyl, D. A. Huse, and C. Monroe, *Many-body localization in a quantum simulator with programmable random disorder*, Nat. Phys. **12**, 907 (2016).
- [50] P. Richerme, Z.-X. Gong, A. Lee, C. Senko, J. Smith, M. Foss-Feig, S. Michalakakis, A. V. Gorshkov, and C. Monroe, *Non-local propagation of correlations in quantum systems with long-range interactions*, Nature (London) **511**, 198 (2014).
- [51] H. Bernien, S. Schwartz, A. Keesling, H. Levine, A. Omran, H. Pichler, S. Choi, A. S. Zibrov, M. Endres, M. Greiner, V. Vuletić, and M. D. Lukin, *Probing many-body dynamics on a 51-atom quantum simulator*, Nature **551**, 579 (2017).
- [52] A. Periwal, E. S. Cooper, P. Kunkel, J. F. Wienand, E. J. Davis, and M. Schleier-Smith, *Programmable interactions and emergent geometry in an array of atom clouds*, Nature **600**, 630 (2021).
- [53] M. K. Joshi, F. Kranzl, A. Schuckert, I. Lovas, C. Maier, R. Blatt, M. Knap, and C. F. Roos, *Observing emergent hydrodynamics in a long-range quantum magnet*, Science **376**, 720 (2022).
- [54] E. H. Lieb and D. W. Robinson, *The finite group velocity of quantum spin systems*, Commun. Math. Phys. **28**, 251 (1972).
- [55] N. Lashkari, D. Stanford, M. Hastings, T. Osborne, and P. Hayden, *Towards the fast scrambling conjecture*, J. High Energy Phys. **2013**, 22 (2013).
- [56] M. Avellino, A. J. Fisher, and S. Bose, *Quantum communication in spin systems with long-range interactions*, Phys. Rev. A **74**, 012321 (2006).
- [57] M. B. Hastings and T. Koma, *Spectral Gap and Exponential Decay of Correlations*, Commun. Math. Phys. **265**, 781 (2006).
- [58] J. Eisert, M. van den Worm, S. R. Manmana, and M. Kastner, *Breakdown of Quasilocality in Long-Range Quantum Lattice Models*, Phys. Rev. Lett. **111**, 260401 (2013).
- [59] P. Hauke and L. Tagliacozzo, *Spread of Correlations in Long-Range Interacting Quantum Systems*, Phys. Rev. Lett. **111**, 207202 (2013).
- [60] M. Foss-Feig, Z.-X. Gong, C. W. Clark, and A. V. Gorshkov, *Nearly Linear Light Cones in Long-Range Interacting Quantum Systems*, Phys. Rev. Lett. **114**, 157201 (2015).
- [61] M. C. Tran, A. Y. Guo, Y. Su, J. R. Garrison, Z. Eldredge, M. Foss-Feig, A. M. Childs, and A. V. Gorshkov, *Locality and Digital Quantum Simulation of Power-Law Interactions*, Phys. Rev. X **9**, 031006 (2019).

- [62] D. J. Luitz and Y. Bar Lev, *Emergent locality in systems with power-law interactions*, Phys. Rev. A **99**, 010105(R) (2019).
- [63] L. Colmenarez and D. J. Luitz, *Lieb-Robinson bounds and out-of-time order correlators in a long-range spin chain*, Phys. Rev. Research **2**, 043047 (2020).
- [64] T. Zhou and X. Chen, *Operator dynamics in a Brownian quantum circuit*, Phys. Rev. E **99**, 052212 (2019).
- [65] T. Kuwahara and K. Saito, *Strictly Linear Light Cones in Long-Range Interacting Systems of Arbitrary Dimensions*, Phys. Rev. X **10**, 031010 (2020).
- [66] M. C. Tran, A. Y. Guo, C. L. Baldwin, A. Ehrenberg, A. V. Gorshkov, and A. Lucas, *Lieb-Robinson Light Cone for Power-Law Interactions*, Phys. Rev. Lett. **127**, 160401 (2021).
- [67] C.-F. Chen and A. Lucas, *Optimal Frobenius light cone in spin chains with power-law interactions*, Phys. Rev. A **104**, 062420 (2021).
- [68] B. Kloss and Y. Bar Lev, *Spin transport in a long-range-interacting spin chain*, Phys. Rev. A **99**, 032114 (2019).
- [69] A. Schuckert, I. Lovas, and M. Knap, *Nonlocal emergent hydrodynamics in a long-range quantum spin system*, Phys. Rev. B **101**, 020416 (2020).
- [70] L. Cevolani, G. Carleo, and L. Sanchez-Palencia, *Spreading of correlations in exactly solvable quantum models with long-range interactions in arbitrary dimensions*, New J. Phys. **18**, 093002 (2016).
- [71] T. Hashizume, S. Kuriyattil, A. J. Daley, and G. Bentsen, *Tunable Geometries in Sparse Clifford Circuits*, arXiv:2202.11750.
- [72] J. Schachenmayer, B. P. Lanyon, C. F. Roos, and A. J. Daley, *Entanglement Growth in Quench Dynamics with Variable Range Interactions*, Phys. Rev. X **3**, 031015 (2013).
- [73] S. Pappalardi, A. Russomanno, B. Žunkovič, F. Iemini, A. Silva, and R. Fazio, *Scrambling and entanglement spreading in long-range spin chains*, Phys. Rev. B **98**, 134303 (2018).
- [74] A. Leroze and S. Pappalardi, *Origin of the slow growth of entanglement entropy in long-range interacting spin systems*, Phys. Rev. Research **2**, 012041(R) (2020).
- [75] T. Kuwahara and K. Saito, *Absence of Fast Scrambling in Thermodynamically Stable Long-Range Interacting Systems*, Phys. Rev. Lett. **126**, 030604 (2021).
- [76] T. Minato, K. Sugimoto, T. Kuwahara, and K. Saito, *Fate of Measurement-Induced Phase Transition in Long-Range Interactions*, Phys. Rev. Lett. **128**, 010603 (2022).
- [77] T. Müller, S. Diehl, and M. Buchhold, *Measurement-Induced Dark State Phase Transitions in Long-Ranged Fermion Systems*, Phys. Rev. Lett. **128**, 010605 (2022).
- [78] R. Bachelard and M. Kastner, *Universal Threshold for the Dynamical Behavior of Lattice Systems with Long-Range Interactions*, Phys. Rev. Lett. **110**, 170603 (2013).
- [79] M. P. Zaletel, R. S. K. Mong, C. Karrasch, J. E. Moore, and F. Pollmann, *Time-evolving a matrix product state with long-ranged interactions*, Phys. Rev. B **91**, 165112 (2015).
- [80] M. A. Nielsen and I. L. Chuang, *Quantum Computation and Quantum Information* (Cambridge University Press, Cambridge, 2000).
- [81] E. Knill, D. Leibfried, R. Reichle, J. Britton, R. B. Blakestad, J. D. Jost, C. Langer, R. Ozeri, S. Seidelin, and D. J. Wineland, *Randomized benchmarking of quantum gates*, Phys. Rev. A **77**, 012307 (2008).
- [82] E. Magesan, J. M. Gambetta, and J. Emerson, *Scalable and Robust Randomized Benchmarking of Quantum Processes*, Phys. Rev. Lett. **106**, 180504 (2011).
- [83] Y. Li, X. Chen, and M. P. A. Fisher, *Quantum Zeno effect and the many-body entanglement transition*, Phys. Rev. B **98**, 205136 (2018).
- [84] M. J. Gullans and D. A. Huse, *Dynamical Purification Phase Transition Induced by Quantum Measurements*, Phys. Rev. X **10**, 041020 (2020).
- [85] S. Sharma, X. Turkeshi, R. Fazio, and M. Dalmonte, *Measurement-induced criticality in extended and long-range unitary circuits*, SciPost Phys. Core **5**, 023 (2022).
- [86] A. Lavasani, Y. Alavirad, and M. Barkeshli, *Measurement-induced topological entanglement transitions in symmetric random quantum circuits*, Nat. Phys. **17**, 342 (2021).
- [87] O. Lunt, M. Szyniszewski, and A. Pal, *Measurement-induced criticality and entanglement clusters: A study of one-dimensional and two-dimensional Clifford circuits*, Phys. Rev. B **104**, 155111 (2021).
- [88] S. Aaronson and D. Gottesman, *Improved simulation of stabilizer circuits*, Phys. Rev. A **70**, 052328 (2004).
- [89] S. Anders and H. J. Briegel, *Fast simulation of stabilizer circuits using a graph-state representation*, Phys. Rev. A **73**, 022334 (2006).
- [90] D. Gottesman, *The Heisenberg Representation of Quantum Computers*, arXiv:quant-ph/9807006
- [91] Note that this expression differs from the usual Heisenberg picture, where the order of  $U$  and  $U^\dagger$  is reversed.
- [92] See supplemental material for details on the structure of the Clifford group, additional numerical results on transport, operator spreading, and entanglement growth in circuits with and without  $U(1)$  symmetry in one and two dimensions, and entanglement dynamics in a long-range Ising chain, including Refs. [93, 94].
- [93] A. D. Córcoles, J. M. Gambetta, J. M. Chow, J. A. Smolin, M. Ware, J. D. Strand, B. L. T. Plourde, and M. Steffen, *Process verification of two-qubit quantum gates by randomized benchmarking*, Phys. Rev. A **87**, 030301(R) (2013).
- [94] R. Koenig and J. A. Smolin, *How to efficiently select an arbitrary Clifford group element*, J. Math. Phys. **55**, 122202 (2014).
- [95] R. Metzler and J. Klafter, *The random walk's guide to anomalous diffusion: a fractional dynamics approach*, Phys. Rep. **339**, 1 (2000).
- [96] V. Zaburdaev, S. Denisov, and J. Klafter, *Lévy walks*, Rev. Mod. Phys. **87**, 483 (2015).
- [97] D. Fattal, T. S. Cubitt, Y. Yamamoto, S. Bravyi, and I. L. Chuang, *Entanglement in the stabilizer formalism*, arXiv:quant-ph/0406168.
- [98] Note that if one were to simulate the dynamics of a state stabilized by  $\pm Z_\ell$  on all lattice sites, i.e., a product state  $|\uparrow\downarrow\cdots\rangle$  in the  $Z$  basis, evolution with respect to  $Z$ -conserving Clifford gates would be entirely classical with  $S(t) = 0$  for all  $t$ . This is in contrast to Haar-random gates with  $U(1)$  symmetry.
- [99] We emphasize again that this corresponds to 1d Hamiltonian systems with couplings  $J \propto r^{-\alpha'}$ , with  $\alpha' = \alpha/2$ .
- [100] P. Zanardi, *Entanglement of quantum evolutions*, Phys. Rev. A **63**, 040304(R) (2001).
- [101] S. Xu and B. Swingle, *Scrambling Dynamics and Out-of-Time Ordered Correlators in Quantum Many-Body Systems: a Tutorial*, arXiv:2202.07060.
- [102] A. Hamma, R. Ionicioiu, and P. Zanardi, *Bipartite entanglement and entropic boundary law in lattice spin systems*, Phys. Rev. A **71**, 022315 (2005).



- [103] Note that the rank has to be calculated by treating the entries  $\nu_\ell^i, \mu_\ell^i$  of  $\mathcal{M}$  as elements of the field  $\mathbb{F}_2$ , i.e., addition and multiplication are performed modulo 2.
- [104] In fact, we find the closest agreement with  $z = 2$  if we make the ansatz  $S(t) \sim t^{1/z} (\log t)^{2/3}$ , from which we obtain  $z = 1.98(1)$ .
- [105] E. Leviatan, F. Pollmann, J. H. Bardarson, D. A. Huse, and E. Altman, *Quantum thermalization dynamics with Matrix-Product States*, arXiv:1702.08894.
- [106] B. Ye, F. Machado, C. D. White, R. S. K. Mong, and N. Y. Yao, *Emergent Hydrodynamics in Nonequilibrium Quantum Systems*, Phys. Rev. Lett. **125**, 030601 (2020).
- [107] T. K. Kivornig, L. Herviou, and J. H. Bardarson, *Time-evolution of local information: thermalization dynamics of local observables*, SciPost Phys. **13**, 080 (2022).
- [108] C. W. von Keyserlingk, F. Pollmann, and T. Rakovszky, *Operator backflow and the classical simulation of quantum transport*, Phys. Rev. B **105**, 245101 (2022).
- [109] T. Farshi, J. Richter, D. Toniolo, A. Pal, and L. Masanes, *Absence of localization in two-dimensional Clifford circuits*, arXiv:2210.10129.
- [110] A. Chandran and C. R. Laumann, *Semiclassical limit for the many-body localization transition*, Phys. Rev. B **92**, 024301 (2015).
- [111] U. Agrawal, A. Zabalo, K. Chen, J. H. Wilson, A. C. Potter, J. H. Pixley, S. Gopalakrishnan, and R. Vasseur, *Entanglement and charge-sharpening transitions in  $U(1)$  symmetric monitored quantum circuits*, arXiv:2107.10279.
- [112] Y. Bao, S. Choi, and E. Altman, *Symmetry enriched phases of quantum circuits*, Ann. Phys. **435**, 168618 (2021).
- [113] S. Zhou, Z. Yang, A. Hamma, and C. Chamon, *Single  $T$  gate in a Clifford circuit drives transition to universal entanglement spectrum statistics*, SciPost Phys. **9**, 087 (2020).
- [114] D. Wei, A. Rubio-Abadal, B. Ye, F. Machado, J. Kemp, K. Srakaew, S. Hollerith, J. Rui, S. Gopalakrishnan, N. Y. Yao, I. Bloch, and J. Zeiher, *Quantum gas microscopy of Kardar-Parisi-Zhang superdiffusion*, Science **376**, 716 (2022).
- [115] R. Islam, R. Ma, P. M. Preiss, M. Eric Tai, A. Lukin, M. Rispoli, and M. Greiner, *Measuring entanglement entropy in a quantum many-body system*, Nature **528**, 77 (2015).
- [116] N. M. Linke, S. Johri, C. Figgatt, K. A. Landsman, A. Y. Matsuura, and C. Monroe, *Measuring the Rényi entropy of a two-site Fermi-Hubbard model on a trapped ion quantum computer* Phys. Rev. A **98**, 052334 (2018).



## SUPPLEMENTAL MATERIAL

### Structure of the Clifford group

Let us provide additional explanations on random Clifford circuits. To begin with, we note that the Pauli group  $\mathcal{P}_L$  on  $L$  qubits is generated by  $L$ -fold tensor products of the Pauli matrices,

$$I = \begin{pmatrix} 1 & 0 \\ 0 & 1 \end{pmatrix}, \quad X = \begin{pmatrix} 0 & 1 \\ 1 & 0 \end{pmatrix}, \quad Y = \begin{pmatrix} 0 & -i \\ i & 0 \end{pmatrix}, \quad Z = \begin{pmatrix} 1 & 0 \\ 0 & -1 \end{pmatrix}. \quad (\text{S1})$$

The Clifford group  $\mathcal{C}_L$  on  $L$  qubits is then defined as the group that preserves the Pauli group  $\mathcal{P}_L$  under conjugation, quotiented by  $U(1)$  to account for a global phase.

#### *Clifford group on 2 qubits*

The two-qubit Clifford group  $\mathcal{C}_2$  can be generated by the gates  $\{P, H, \text{CNOT}_{0,1}\}$ , where

$$P = \begin{pmatrix} 1 & 0 \\ 0 & i \end{pmatrix}, \quad H = \begin{pmatrix} 1 & 1 \\ 1 & -1 \end{pmatrix}, \quad \text{CNOT}_{0,1} = \begin{pmatrix} 1 & 0 & 0 & 0 \\ 0 & 1 & 0 & 0 \\ 0 & 0 & 0 & 1 \\ 0 & 0 & 1 & 0 \end{pmatrix}, \quad \text{CNOT}_{1,0} = \begin{pmatrix} 1 & 0 & 0 & 0 \\ 0 & 0 & 0 & 1 \\ 0 & 0 & 1 & 0 \\ 0 & 1 & 0 & 0 \end{pmatrix}. \quad (\text{S2})$$

For convenience we further define the composite gates  $W$  and  $V$ ,

$$W = H \cdot P, \quad V = W \cdot W = H \cdot P \cdot H \cdot P. \quad (\text{S3})$$

The two-qubit Clifford group can then be structured into different classes, characterized by their number of two-qubit gates [S1]. The first class contains solely single-qubit gates,

$$(h_0 \otimes h_1)(v_0 \otimes v_1)(p_0 \otimes p_1), \quad \text{with } h_i \in \{I, H\}, \quad v_i \in \{I, V, W\} \text{ and } p_i \in \{I, X, Y, Z\}, \quad (\text{S4})$$

which results in  $2^2 \times 3^2 \times 4^2 = 24^2 = 576$  distinct gates. The second class requires one CNOT gate,

$$(h_0 \otimes h_1)(v_0 \otimes v_1)\text{CNOT}_{0,1}(v'_0 \otimes v'_1)(p_0 \otimes p_1), \quad \text{with } h_i \in \{I, H\}, \quad v_i, v'_i \in \{I, V, W\}, \quad p_i \in \{I, X, Y, Z\}, \quad (\text{S5})$$

which contains  $2^2 \times 3^2 \times 3^2 \times 4^2 = 5184$  gates. The third class comprises sequences with two CNOT gates,

$$(h_0 \otimes h_1)(v_0 \otimes v_1)\text{CNOT}_{0,1}\text{CNOT}_{1,0}(v'_0 \otimes v'_1)(p_0 \otimes p_1), \quad \text{with } h_i \in \{I, H\}, \quad v_i, v'_i \in \{I, V, W\}, \quad p_i \in \{I, X, Y, Z\}, \quad (\text{S6})$$

which yields  $2^2 \times 3^2 \times 3^2 \times 4^2 = 5184$  gates. Eventually, the fourth class requires three CNOT gates,

$$(h_0 \otimes h_1)(v_0 \otimes v_1)\text{CNOT}_{0,1}\text{CNOT}_{1,0}\text{CNOT}_{0,1}(p_0 \otimes p_1), \quad \text{with } h_i \in \{I, H\}, \quad v_i \in \{I, V, W\}, \quad p_i \in \{I, X, Y, Z\}, \quad (\text{S7})$$

which contains  $2^2 \times 3^2 \times 4^2 = 576$  gates. In total, there are thus 11520 distinct 2-qubit Clifford gates.

In practice, these 11520 distinct gates can be stored in a look-up table. Every application of a two-qubit Clifford gate in the circuit then corresponds to selecting and carrying out a random element of the look-up table. Alternatively, another useful approach to randomly select an element of  $\mathcal{C}_2$  has been presented in [S2]. In essence, it consists of generating a suitable symplectic matrix, which upon multiplication with the stabilizer tableau, implements the action of a random gate. This approach is particularly beneficial if one is interested in Clifford gates on more than two qubits since  $|\mathcal{C}_{n>2}|$  is too large to be stored in a look-up table. In this paper, we use both approaches complementarily.

#### *2-qubit Clifford gates that conserve $\langle \psi(t) | Z_1 + Z_2 | \psi(t) \rangle$*

In this paper, we are mainly interested in the interplay between transport and entanglement growth. To this end, we consider circuits with  $U(1)$  symmetry that conserve the total Pauli- $Z$  component, such that magnetization exhibits hydrodynamic transport. Given the decomposition of the full two-qubit Clifford group in Eqs. (S4) - (S7), the Clifford gates that conserve magnetization can be written as follows. The first class consists of single-qubit gates,

$$(h_0 \otimes h_1)(p_0 \otimes p_1), \quad \text{with } h_i \in \{I, P\}, \text{ and } p_i \in \{I, Z\}, \quad (\text{S8})$$

and contains  $2^2 \times 2^2 = 4^2 = 16$  distinct gates. The second class requires one CNOT gates,

$$(h_0 \otimes h_1) \text{CNOT}_{0,1}(I \otimes W)(p_0 \otimes p_1), \text{ with } h_0 \in \{I, P\}, h_1 \in \{V, H\}, p_i \in \{I, Z\}, \quad (\text{S9})$$

and contains  $2 \times 2 \times 2^2 = 16$  distinct gates. The third class requires two CNOT gates,

$$(h_0 \otimes h_1) \text{CNOT}_{0,1} \text{CNOT}_{1,0}(I \otimes W)(p_0 \otimes p_1), \text{ with } h_0 \in \{H, V\}, h_1 \in \{I, P\}, p_i \in \{I, Z\}, \quad (\text{S10})$$

and contains  $2 \times 2 \times 2^2 = 16$  gates. Finally, the fourth class requires three CNOT gates,

$$(h_0 \otimes h_1) \text{CNOT}_{0,1} \text{CNOT}_{1,0} \text{CNOT}_{0,1}(p_0 \otimes p_1), \text{ with } h_i \in \{I, P\}, p_i \in \{I, Z\}, \quad (\text{S11})$$

and contains  $2^2 \times 2^2 = 16$  gates. Thus, there are 64 distinct 2-qubit Clifford gates which conserve the magnetization  $\langle \psi(t) | Z_1 + Z_2 | \psi(t) \rangle$ . We note that this is distinctly smaller than the size of the full two-qubit Clifford group,  $64 \ll |\mathcal{C}_2| = 11520$ . Moreover, regarding the production of entanglement, let us note that in the full two-qubit Clifford group only 576 gates are separable [Eq. (S4)], which corresponds to a fraction of  $576/11520 = 0.05$ . In contrast, in the case of gates that conserve magnetization,  $16/64 = 0.25$  gates are separable [Eq. (S8)]. Thus, if one considers Clifford circuits with U(1) symmetry, the application of a random gate will, on average, produce less entanglement compared to Clifford circuits without conservation law. This has the effect that, even in regimes where the dynamical critical exponent is the same for symmetric and asymmetric circuits, symmetric circuits will typically take longer (by some  $\mathcal{O}(1)$  factor) to reach the steady-state value than asymmetric circuits.

It is also instructive to study the action of the U(1)-symmetric Clifford gates in Eqs. (S8) - (S11) on Pauli operators,  $\mathcal{U}(\mathcal{O}_1 \otimes \mathcal{O}_2) \mathcal{U}^\dagger$ . Given two lattice sites, as well as the Pauli and identity operators in Eq. (S1), there are  $2^4$  different configurations to consider. First of all, it is obvious that with probability  $p = 1$ ,

$$I \otimes I \longrightarrow I \otimes I \quad (p = 1), \quad (\text{S12})$$

i.e., given identity operators on both lattice sites, this configuration remains unchanged for all 64 possible U(1)-symmetric Clifford gates. This result naturally holds for Clifford gates without conservation law as well. Crucially, for other nontrivial initial operator configurations, the effect of the U(1) conservation law becomes apparent. In particular, we have,

$$\left. \begin{array}{l} Z \otimes \mathbb{1} \\ \mathbb{1} \otimes Z \end{array} \right\} \longrightarrow \left\{ \begin{array}{l} Z \otimes \mathbb{1} \quad (p = 1/2) \\ \mathbb{1} \otimes Z \quad (p = 1/2) \end{array} \right\}, \quad Z \otimes Z \longrightarrow Z \otimes Z \quad (p = 1), \quad (\text{S13})$$

which highlights the fact that a single  $Z$  operator can perform jumps between different lattice sites, but no other operators are created in the process. As a consequence, if one starts with an isolated  $Z$  operator, the application of U(1)-symmetric Clifford gates will lead to a random-walk of the  $Z$  operator, but the operator string will remain of length one throughout the entire circuits.

In contrast, if the initial configuration contains solely  $X$  or  $Y$  operators, the U(1)-symmetric Clifford gates cannot produce new  $Z$  operators,

$$\left. \begin{array}{l} X \otimes X \\ Y \otimes Y \\ X \otimes Y \\ Y \otimes X \end{array} \right\} \longrightarrow \left\{ \begin{array}{ll} X \otimes X & (p = 1/4) \\ Y \otimes Y & (p = 1/4) \\ X \otimes Y & (p = 1/4) \\ Y \otimes X & (p = 1/4) \end{array} \right\}. \quad (\text{S14})$$

Finally, the remaining 8 configurations transform according to,

$$\left. \begin{array}{l} X \otimes \mathbb{1} \\ \mathbb{1} \otimes X \\ Y \otimes \mathbb{1} \\ \mathbb{1} \otimes Y \\ X \otimes Z \\ Z \otimes X \\ Y \otimes Z \\ Z \otimes Y \end{array} \right\} \longrightarrow \left\{ \begin{array}{ll} X \otimes \mathbb{1} & (p = 1/8) \\ \mathbb{1} \otimes X & (p = 1/8) \\ Y \otimes \mathbb{1} & (p = 1/8) \\ \mathbb{1} \otimes Y & (p = 1/8) \\ X \otimes Z & (p = 1/8) \\ Z \otimes X & (p = 1/8) \\ Y \otimes Z & (p = 1/8) \\ Z \otimes Y & (p = 1/8) \end{array} \right\}. \quad (\text{S15})$$

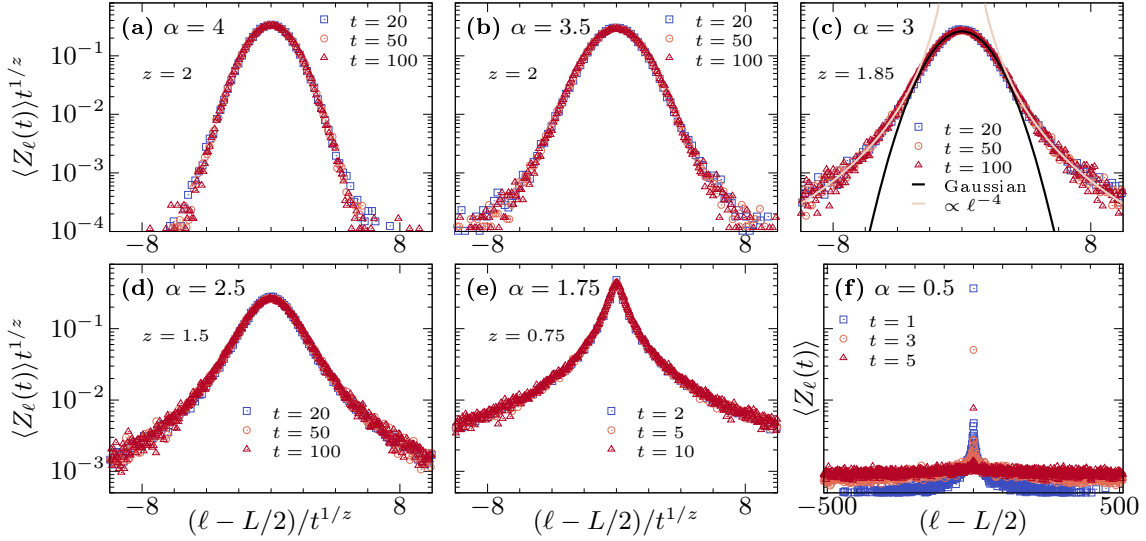


FIG. S1. [(a)-(e)] Rescaled density profile  $\langle Z_\ell(t) \rangle t^{1/z}$  versus  $(\ell - L/2)/t^{1/z}$  in long-range circuits with different values of  $\alpha$ . For  $\alpha = 3$ , we observe that while the bulk is well described by a Gaussian, the distribution exhibits heavy tails  $\propto \ell^{-4}$ . (f)  $\langle Z_\ell(t) \rangle$  versus  $\ell - L/2$  in circuits with  $\alpha = 0.5$ . The system thermalizes in a few time steps, resulting in a flat distribution.

These update rules for two-site Pauli operators under the action of U(1)-symmetric Clifford gates also allows an understanding of our finding in the context of Figs. 3 (d)-(f). In particular, starting with an isolated  $X$  operator, with probability  $p = 4 \times 1/8 = 1/2$ , a  $Z$  operator is created by the first Clifford gate acting on  $X \otimes I$ . Since this  $Z$  operator remains conserved when a gate acts on  $Z \otimes I$  [cf. Eq. (S13)], and since the initial operator string contains many  $I$  operators, it is highly probable that more  $Z$  operators are created due to Eq. (S15) and these  $Z$  operators then dominate the spreading of the light cone.

### Additional data on hydrodynamics and operator spreading in long-range 1d Clifford circuits

#### Transport properties

In addition to the data presented in Fig. 2 in the main text, we provide further numerical results on transport in long-range Clifford circuits in Fig. S1. We emphasize that this data can be understood as resulting from the time evolution of an initial state of the form  $|\psi(0)\rangle = |\rightarrow\rangle^{\otimes L/2-1} |\uparrow\rangle |\rightarrow\rangle^{\otimes L/2}$ . However, due to the particular nature of U(1)-symmetric Clifford gates, i.e., the fact that the stabilizer  $\mathcal{O}_i = Z_{L/2}$  will remain of length one throughout the entire circuit, it is in fact not necessary to study  $|\psi(t)\rangle$ , but just to keep track of the random walk  $\mathcal{U}Z_\ell\mathcal{U}^\dagger$  of the isolated  $Z$  operator. Averaging over many random circuit realizations yields the expectation value  $\langle Z_\ell(t) \rangle$ .

In Fig. S1 (a)-(e), the rescaled expectation value  $\langle Z_\ell(t) \rangle t^{1/z}$  is plotted versus  $(\ell - L/2)/t^{1/z}$  for fixed times  $t$  and different values of  $\alpha$ . Generally, we find a convincing agreement with the theoretical Lévy-flight prediction [Eq. (2) in main text]. In particular, we observe approximate Gaussian profiles for  $\alpha > 3$  that collapse for the diffusive value  $z = 2$ . Moreover, for  $1 < \alpha < 3$ , the profile becomes non-Gaussian with a pronounced peak at  $\ell = L/2$  and collapses for  $z = \alpha - 1$ .

Let us now comment on  $\alpha = 3$  [Fig. S1 (c)]. In contrast to the prediction of  $z = 2$ , we find that the numerically obtained value  $z \approx 1.85$  yields a much more convincing data collapse. These discrepancies might be due to finite-size and finite-time effects, which we expect to be most pronounced at the phase boundary. Furthermore, while the bulk of  $\langle Z_\ell(t) \rangle$  is well described by a Gaussian, consistent with the emergence of diffusive transport for  $\alpha \geq 3$ , we observe that  $\langle Z_\ell(t) \rangle$  exhibits heavy non-Gaussian tails decaying as  $\propto \ell^{-4}$ , which are well-known to occur for Lévy flights [S5]. It would be interesting to understand in more detail the potential impact of such tails on the dynamics of entanglement  $S(t)$  discussed in Fig. 4. In particular, as shown in Fig. S2, the operator spreading quantified by  $\rho(\ell, t)$  likewise develops such non-Gaussian tails. Let us note that for larger values of  $\alpha$ , such as  $\alpha = 5$  considered in Fig. 2 (c) in the main text, the density distribution is well described by a Gaussian without heavy tails (at least within the limitations set by the statistical fluctuations).

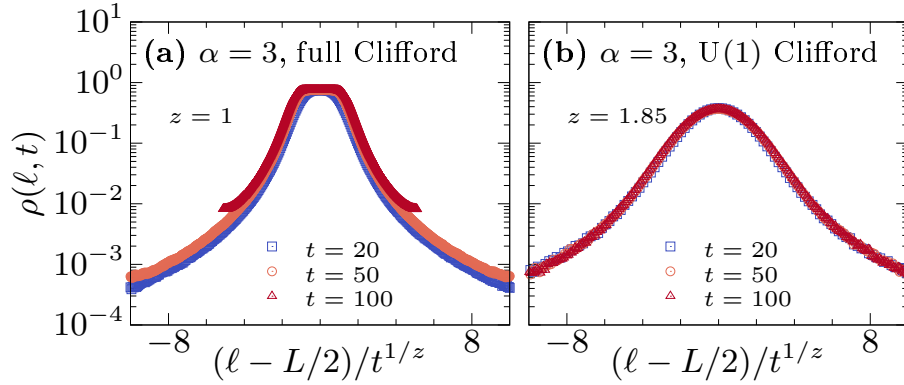


FIG. S2. Circuit-averaged  $\rho(\ell, t)$  versus rescaled variable  $(\ell - L/2)/t^{1/z}$ , obtained analogous to Fig. 3 of the main text. Data is shown for circuits with  $L = 1024$  and  $\alpha = 3$  for (a) Clifford gates without conservation law and (b) U(1)-symmetric gates.

Eventually, in Fig. S1 (f), we show  $\langle Z_\ell(t) \rangle$  obtained in highly non-local circuits with  $\alpha = 0.5$ . Consistent with the absence of a hydrodynamic tail of  $\langle Z_{L/2}(t) \rangle$ , cf. Fig. 2 (e), we find that the single  $Z$  excitation spreads over the entire system within a few time steps, resulting in a flat distribution.

#### Operator spreading

To proceed, we also provide additional data on the operator spreading  $\mathcal{U}X_{L/2}\mathcal{U}^\dagger$  of an initially isolated  $X$  operator, analogous to Fig. 3 of the main text. In Fig. S2 (a) and (b), we focus on  $\alpha = 3$  and show cuts of  $\rho(\ell, t)$  (see definition in main text) at fixed times for Clifford circuits without conservation law as well as circuits with U(1)-symmetric gates. In the former case [Fig. S2 (a)], we find that  $\rho(\ell, t)$  approximately collapses for  $z = 1$ . Moreover, for the longest time  $t = 100$  shown here,  $\rho(\ell, t)$  exhibits a flat plateau around  $\ell = L/2$  at the saturation value  $\rho(\ell, t) = 0.75$ , which indicates full scrambling within this area. In the latter case [Fig. S2 (b)], we find that  $\rho(\ell, t)$  is similar to the density profiles  $\langle Z_\ell(t) \rangle$  in Fig. S1 (c), with a Gaussian shape in the bulk and additional heavy tails. Moreover, as in Fig. S1 (c), we find a data collapse for  $z \approx 1.85$ . As discussed in the main text, this similarity of  $\langle Z_\ell(t) \rangle$  and  $\rho(\ell, t)$  is expected in U(1)-symmetric circuits since  $\mathcal{O}(t)$  will quickly be dominated by  $Z$  operators such that the operator spreading will be impacted by the hydrodynamic behavior of the conserved quantity. Moreover, we note that the value of  $z \approx 1.85$  seems consistent with the growth of entanglement discussed in Fig. 4, where we found deviations from the theoretically expected  $z = 2$  at  $\alpha = 3$ . We here leave it to future work to study finite-size and finite-time effects in more details (but see Figs. S5 and S6) and to analyze the potential impacts of the non-Gaussian tails on  $S(t)$ .

While the operator string  $\mathcal{O}(t)$  will quickly be dominated by  $Z$  operators in the case of U(1)-symmetric Clifford gates, it is interesting to study how  $X$  and  $Y$  operators spread within  $\mathcal{O}(t)$ . Even though their overall weight decays as  $\propto t^{-1/z}$  [see inset in Fig. 3 (f) in the main text] their dynamics might differ from the hydrodynamic behavior of the  $Z$  operators. To this end, we analyze in Fig. S3 (c) the spreading of  $X$  and  $Y$  operators in terms of the quantity,

$$\rho_{x,y}(\ell, t) = \sum_{\sigma=x,y} \rho_\sigma(\ell, t) = \sum_{\sigma=x,y} \text{tr}[\mathcal{O}_\ell(t)\Sigma^\sigma]/2, \quad (\text{S16})$$

where, in contrast to  $\rho(\ell, t)$ , the sum now runs only over  $X$  and  $Y$  operators. [As already stated in the main text,  $\mathcal{O}_\ell(t)$  denotes the local Pauli or identity matrix at the  $\ell$ th position of the operator string and  $\Sigma^{\sigma=x,y,z} = \{X, Y, Z\}$ . Given the orthogonality of Pauli matrices, we have  $\text{tr}(\mathcal{O}_\ell(t)\Sigma^\sigma)/2 = \delta_{\mathcal{O}_\ell(t), \Sigma^\sigma}$ .] Focusing on  $\alpha = 5$ , we find in Fig. S3 (c) that  $\rho_{x,y}(\ell, t)$  spreads diffusively and is qualitatively very similar to our results for  $\rho(\ell, t)$  in U(1)-symmetric circuits in the main text. This is highlighted by comparing to Fig. S3 (b), where we show  $\rho(\ell, t)$  (i.e., including  $Z$  operators) for the same system size  $L = 128$ . Thus, it appears that not only is the overall number of  $X$  and  $Y$  operators reduced [cf. Fig. 3 (f)], but the spreading of  $X$  and  $Y$  operators is also affected by the presence of the conservation law. This fact is further emphasized by comparing the results for  $\rho_{x,y}(\ell, t)$  in Fig. S3 (c) to the case of full Clifford circuits without conservation law in Fig. S3 (a) (here  $\rho(\ell, t)$  and  $\rho_{x,y}(\ell, t)$  are equivalent as no operator is favored), where the spreading is ballistic. Let us note that this slow spreading of  $X$  and  $Y$  operators in U(1)-symmetric Clifford circuits shown in Fig. S3 (c) appears to differ to more generic Haar-random circuits with conservation law, where conserved operators



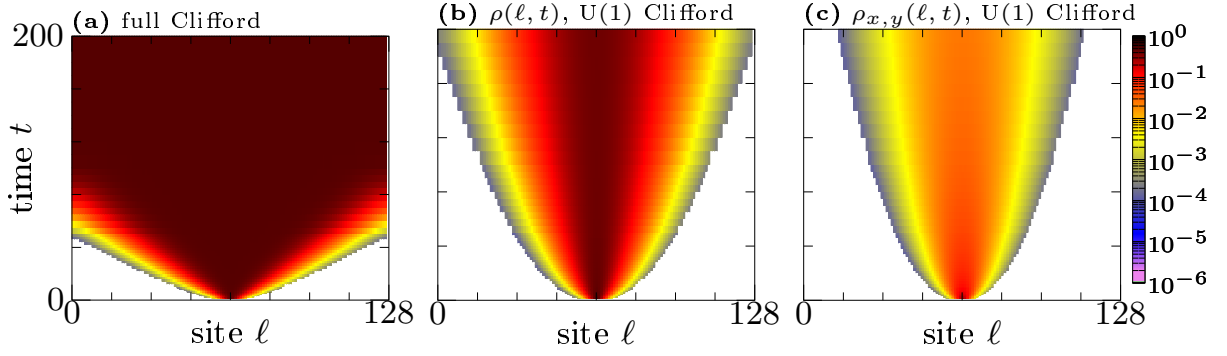


FIG. S3. Operator spreading resulting from  $\mathcal{O}(0) = X_{L/2}$  in Clifford circuits with  $L = 128$  and  $\alpha = 5$ . (a)  $\rho(\ell, t)$  under full Clifford evolution without conservation law. (b)  $\rho(\ell, t)$  in U(1)-symmetric Clifford circuits. Note that data in panels (a) and (b) is analogous to data for  $L = 1024$  shown in Figs. 3 (a) and (d) in the main text. (c)  $\rho_{x,y}(\ell, t)$  [Eq. (S16)] in U(1)-symmetric circuits.

yield a slow hydrodynamic bulk that lags behind the significantly faster spreading front dominated by nonconserved operators [S3].

Let us now provide some additional analysis regarding the dynamics of the total support  $\rho_{\text{tot}}(t)$ , already considered in Figs. 3 (c) and (f) in the main text. In particular, in Figs. S4 (a) and (b), we show  $\rho_{\text{tot}}(t)$  for different  $\alpha$  values in circuits without and with conservation law and two system sizes  $L = 1024, 2048$ . Comparing the curves for different  $L$ , we find that especially for larger values of  $\alpha$ , finite-size effects are well-controlled on the time scales shown here. To study the growth of  $\rho_{\text{tot}}(t)$  in more detail, Figs. S4 (c) and (d) show its logarithmic derivative. While for large  $\alpha = 5$  we recover ballistic behavior ( $d \log \rho_{\text{tot}}(t)/d \log t \rightarrow 1$ ) in the unsymmetric case and diffusive growth ( $d \log \rho_{\text{tot}}(t)/d \log t \rightarrow 0.5$ ) in U(1)-symmetric circuits, we find that the two gate sets behave drastically different at lower  $\alpha$ . Specifically, for unsymmetric circuits with  $\alpha \lesssim 2$  we are unable to find an extended window with constant  $d \log \rho_{\text{tot}}(t)/d \log t$ , indicating that  $\rho_{\text{tot}}(t)$  is not described by a power law anymore. While this seems consistent with the phase diagram for long-range systems obtained in [S4], where it was argued that the nature of operator spreading changes for  $\alpha \leq 2$ , we cannot exclude the impact of finite-size/finite-time effects which are clearly more pronounced for smaller  $\alpha$ . Interestingly, in contrast to full Clifford evolution, we find that the growth of  $\rho_{\text{tot}}(t)$  in U(1)-symmetric circuits appears to be described by a power law for all values of  $\alpha$  shown here, with approximately constant  $d \log \rho_{\text{tot}}(t)/d \log t$  over an extended time window [Fig. S4 (d)]. Surprisingly, however, we find that the growth of  $\rho_{\text{tot}}(t)$  never exceeds ballistic  $\propto t$  behavior even for small  $\alpha$ , which is somewhat unexpected as the dynamical transport exponent  $z$  continues to decrease for  $\alpha < 2$ , cf. Fig. 1 (b) in the main text.

In addition to the total support  $\rho_{\text{tot}}(t)$  of  $\mathcal{O}(t)$ , it is instructive to study the left and right endpoints  $\rho_L(t)$ ,  $\rho_R(t)$  of the operator string, see also Fig. 4 in the main text,

$$\rho_L(t) = \min\{\ell \mid \text{tr}[\mathcal{O}_\ell(t)\Sigma^{x,y,z}] \neq 0\} \ , \quad \rho_R(t) = \max\{\ell \mid \text{tr}[\mathcal{O}_\ell(t)\Sigma^{x,y,z}] \neq 0\} \ , \quad (\text{S17})$$

which are defined as the smallest and largest lattice site  $\ell$ , for which  $\mathcal{O}(t)$  is a non-identity Pauli matrix. For the initial condition  $\mathcal{O}(0) = X_{L/2}$ , we obviously have  $\rho_L(t) = \rho_R(t) = L/2$ . For  $t > 0$ , the difference  $|\rho_L(t) - \rho_R(t)|$  is expected to grow. In Figs. S4 (e) and (f),  $|\rho_L(t) - \rho_R(t)|/L$  is shown for circuits without and with conservation law and different values of  $\alpha$ . While for  $\alpha = 5$  we recover ballistic  $\propto t$  or diffusive  $\propto t^{1/2}$  behavior respectively, the growth of  $|\rho_L(t) - \rho_R(t)|$  appears to become more and more similar for smaller  $\alpha$ . Specifically, considering  $\alpha = 1.5$ , we approximately find  $|\rho_L(t) - \rho_R(t)| \propto t^{1.5}$  for unsymmetric circuits, while  $|\rho_L(t) - \rho_R(t)| \propto t^{1.3}$  for circuits with U(1) symmetry. While we should note that it is rather tricky to fit a power law given the short time scales for such small  $\alpha$ , the overall behavior in Figs. S4 (e) and (f) appears at least consistent with our observation that entanglement dynamics  $S(t)$  becomes almost unaffected by the presence of a conservation law once  $\alpha$  is sufficiently small, cf. Fig. 4 in the main text.

Comparing the data of  $\rho_{\text{tot}}(t)$  in Figs. S4 (a) and (b) with the results for  $|\rho_L(t) - \rho_R(t)|$  in Figs. S4 (e) and (f), we conclude that although the shape of the light cones may become similar for circuits with and without conservation law if  $\alpha$  is small, the interior of the light cone behaves notably different. In particular, the comparatively slower growth of  $\rho_{\text{tot}}(t)$  in U(1)-symmetric circuits suggests that the operator string  $\mathcal{O}(t)$  still contains a larger fraction of identity operators [and as we discussed in Fig. 3 (f), many more  $Z$  operators than  $X$  and  $Y$ ], whereas in circuits without conservation law one quickly approaches the equilibrium distribution where  $X$ ,  $Y$ ,  $Z$ , and identity operators all occur

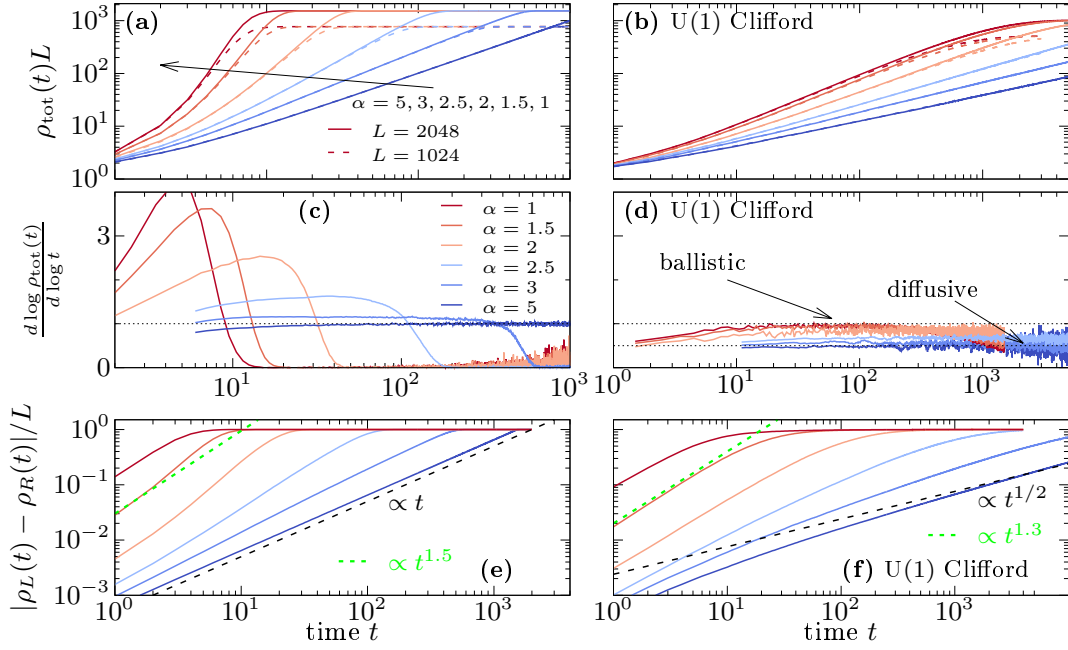


FIG. S4. (a) Total support  $\rho_{\text{tot}}(t)L$  of  $\mathcal{O}(t)$  for  $L = 1024, 2048$  and different values of  $\alpha$  (arrow), resulting from isolated operator  $\mathcal{O}(0) = X_{L/2}$  under full Clifford evolution without conservation law. Note that data is analogous to Fig. 3 (c) in the main text. (c) Logarithmic derivative  $d \log \rho_{\text{tot}}(t)/d \log t$  of the data in panel (a). (e) Normalized difference  $|\rho_L(t) - \rho_R(t)|/L$  between left and right endpoint of  $\mathcal{O}(t)$ , cf. Eq. (S17). Panels (b), (d), and (f) show analogous data, but now for Clifford circuits with U(1)-symmetric gates.

with probability  $1/4$ .

### Finite-size scaling of the dynamical exponent $z$

In this section we explain the procedure we use for estimating the magnitude of finite-size effects in our estimates of the dynamical critical exponent  $z$  from the entanglement data. This is necessitated by the fact that we observe fairly significant drifts with system size in our estimates of  $z$ , even at the large system sizes  $L \sim 10^3$  accessible with Clifford circuits. In passing, we note that it may be the case that Clifford circuits exhibit larger finite-size effects than less structured models, such as Haar-random circuits. It would be interesting to understand better whether the much larger system sizes accessible with Clifford circuits compensate for any larger propensity for significant finite-size effects.

To extract  $z$  from the entanglement growth, first for each system size  $L$  we calculate the ‘saturation time’  $t_{\text{sat}}$ , which for practical purposes we define to be the smallest time at which  $S_{L/2}(t)$  is within 1% of its steady-state value. Assuming the entanglement growth is dominated by the asymptotic scaling  $S(t) \sim t^{1/z}$ —which empirically is what we observe—and using the fact that the steady-state entanglement is  $\mathcal{O}(L)$ , the saturation time should scale as  $t_{\text{sat}} \sim L^z$ . Thus for a given set of system sizes  $\{L_i\}$ , we can estimate  $z$  using a linear fit of  $\log t_{\text{sat}}$  vs  $\log L$ .

To account for finite-size effects, we artificially restrict the dataset we use for this fit to system sizes  $L \leq L_{\text{end}}$  for some maximum  $L_{\text{end}}$ , obtaining a corresponding estimate  $z(L_{\text{end}})$ . We then vary  $L_{\text{end}}$  from  $L_{\text{end}} = 128$  to the largest system size available, typically  $L_{\text{end}} = 1024$  or  $2048$  depending on the value of  $\alpha$ .

Having obtained a range of estimates  $\{z(L_{\text{end}})\}$  for different values of  $L_{\text{end}}$ , we perform an initial fit of these estimates to a power-law,  $z(L_{\text{end}}) = b(x_0 + 1/L_{\text{end}})^{-a}$ . In principle this initial fit can be used to perform the extrapolation of  $z$  as  $1/L_{\text{end}} \rightarrow 0$ . However, this may give undue weight to this particular power-law fit, since the extrapolated value at 0 can depend somewhat sensitively on the parameters of the fit. To account for this, we perform a form of ‘least squares Monte Carlo’, over a parameter space centered around the parameters obtained from the initial fit. We randomly draw a set of parameters  $\mathbf{p} = (a, b, x_0)$  with probability proportional to the inverse square of the least squares cost function  $\epsilon(\mathbf{p}) = \sum_i (y_{\mathbf{p}}(x_i) - y_i)^2 / \sigma_i^2$ , where  $y_{\mathbf{p}}(x_i) = b(x_0 + x_i)^{-a}$ , and the data  $(x_i, y_i, \sigma_i)$  are the values of  $1/L_{\text{end}}$ , the corresponding estimates  $z(L_{\text{end}})$ , and their errors. For each set of parameters  $\mathbf{p}$  we obtain an estimate of the extrapolated value at  $1/L_{\text{end}} = 0$ . To get our final estimate of  $z$ , we draw  $10^5$  Monte Carlo samples, and take the

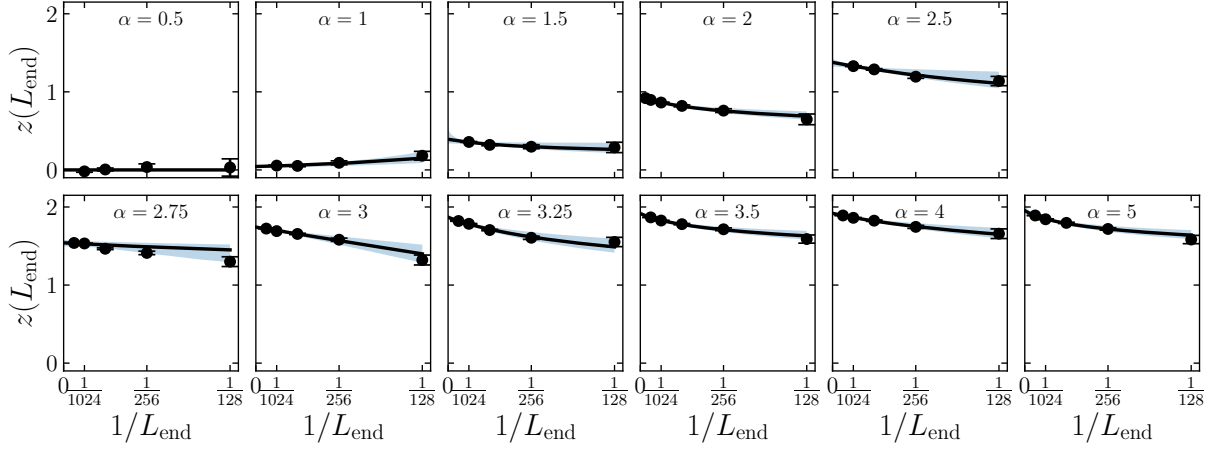


FIG. S5. Extrapolation procedure for the dynamical critical exponent  $z$  in U(1)-symmetric Clifford circuits, for different values of  $\alpha$ . Data points come from estimates using a linear fit of  $\log t_{\text{sat}}$  vs  $\log L$ , while the black line is the median fit from the ‘least squares Monte Carlo’ procedure described in the main text, and the shaded blue area is the corresponding 95% confidence interval. In most cases the trend as  $1/L_{\text{end}} \rightarrow 0$  is for the  $z$  estimate to increase, except at  $\alpha = 1$ , where the estimate decreases towards zero, and  $\alpha = 0.5$ , where the estimate remains very close to zero.

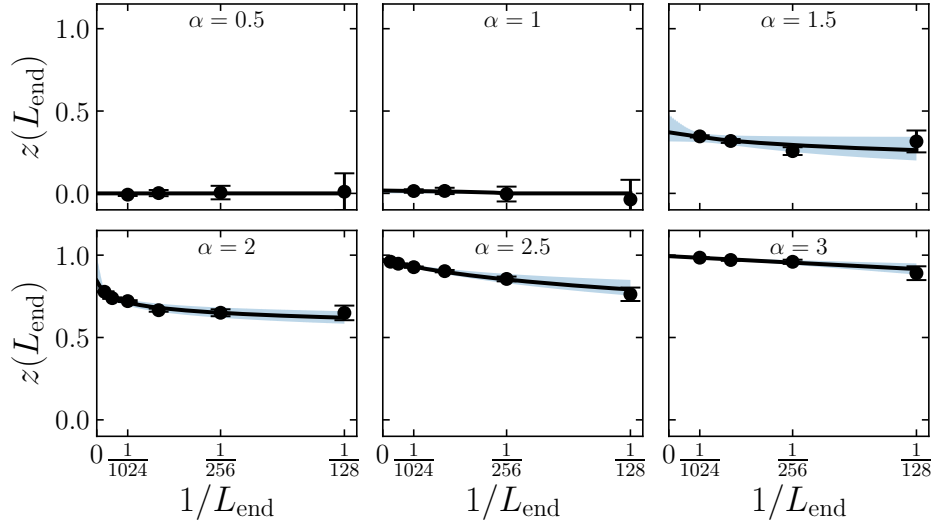


FIG. S6. Extrapolation procedure for the dynamical critical exponent  $z$  in asymmetric Clifford circuits, for different values of  $\alpha$ . Data points come from estimates using a linear fit of  $\log t_{\text{sat}}$  vs  $\log L$ , while the black line is the median fit from the ‘least squares Monte Carlo’ procedure described in the main text, and the shaded blue area is the corresponding 95% confidence interval.

median extrapolated value. The lower and upper error bars are given by the values of  $z$  at which 2.5% and 97.5% respectively of the extrapolated values are below these thresholds.

These extrapolation procedures are shown in Figs. S5 and S6 for U(1)-symmetric and asymmetric Clifford circuits respectively. In most cases the trend as  $1/L_{\text{end}} \rightarrow 0$  is for the  $z$  estimate to increase, except for U(1)-symmetric circuits at  $\alpha = 1$ , where the estimate decreases towards zero, and for the same circuits at  $\alpha = 0.5$ , where the estimate remains very close to zero. We note that the uncertainty in the estimate seems to be larger around  $\alpha \approx 3$ , where the transition occurs from short- to long-range behavior. As discussed in the main text, this may be related to the fact that both  $\langle Z_\ell(t) \rangle$  and  $\rho(\ell, t)$  develop heavy non-Gaussian tails at  $\alpha \approx 3$  (see Fig. S1). We defer further investigation of this relationship to future work.

### Comparison between long-ranged circuits and circuits with nearest-neighbor gates

For sufficiently large  $\alpha$ , the properties of circuits with long-range interactions approach those of strictly local circuits. This fact is demonstrated in Fig. S7, where we compare transport and entanglement growth in long-range circuits with  $\alpha = 5$  and circuits with nearest-neighbor gates. As shown in Fig. S7 (a), the spin excitation  $\langle Z_{L/2}(t) \rangle$  decays diffusively  $\propto t^{-1/2}$  for both circuit variants and the data for the two different circuits agree very well with each other. Likewise, the entanglement production in long-range circuits with  $\alpha = 5$  is essentially equivalent to that in local circuits. In particular, we find that  $S(t)$  growth diffusively  $\propto t^{1/2}$  at long times for circuits with U(1) conservation law, and linearly  $\propto t$  for circuits without charge conservation.

### Comparison between random Clifford circuits and Haar-random circuits

Let us briefly compare entanglement dynamics in Clifford circuits to the case of Haar-random circuits. Such a comparison is shown in Fig. S8 (a) for circuits without conservation law and in Fig. S8 (b) for circuits with U(1)-symmetric gates. We here focus on  $\alpha = 2$  and  $\alpha = 5$  and show data for three different systems sizes  $L = 14, 16, 18$  (note that in contrast to Clifford circuits, the simulation of Haar-random circuits is exponentially costly in  $L$ ). While for Clifford circuits all Rényi entropies are equivalent, we show  $S_2(t)$  in the case of Haar-random gates.

On one hand, for the case without conservation law, we find that the entanglement dynamics is very similar for Clifford and Haar-random circuits, which emphasizes the fact that random Clifford circuits form unitary 2-designs and can imitate the properties of more generic types of unitary evolution. On the other hand, in the U(1)-symmetric case, we find that the dynamics of  $S(t)$  is again qualitatively similar in Clifford and Haar-random circuits, but  $S(t)$  appears to saturate slightly faster towards its steady-state value for Haar-random gates. As already discussed in the context of Eqs. (S8)-(S11), we attribute this difference to the fact that the set of U(1)-symmetric Clifford gates contains a comparatively high percentage of separable gates that generate no entanglement. We expect, however, that this will not change the dynamical critical exponent  $z$ , but only affect the coefficient of the  $S(t) \propto t^{1/z}$  scaling. In particular, in the thermodynamic limit  $L \rightarrow \infty$ , we expect that the dynamics of  $S(t)$  in U(1)-symmetric Clifford circuits at finite times is representative of the dynamics of higher Rényi entropies  $S_{n>1}(t)$  in more generic quantum many-body systems.

### Entanglement dynamics in long-range quantum many-body systems

To further support the generality of our conclusions of Fig. 4 in the main text, let us now consider an actual chaotic quantum many-body system. Specifically, we show in Fig. S9 the growth of the Rényi- $\infty$  entropy  $S_\infty(t)$  of the long-range tilted field Ising model [S6, S7], with

$$H = \sum_{i < j} \frac{J}{|i - j|^{\alpha'}} Z_i Z_j + \sum_i h_z Z_i + h_x X_i - J(Z_1 + Z_L), \quad (\text{S18})$$

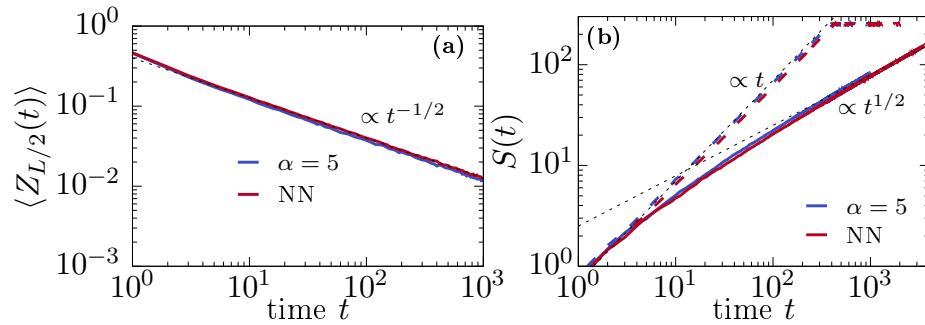


FIG. S7. (a)  $\langle Z_{L/2}(t) \rangle$  for long-range circuits with  $\alpha = 5$  and circuits with nearest-neighbor (NN) gates, obtained analogous to Fig. 2 in the main text. (b) Corresponding entanglement growth in circuits with U(1) conservation law (solid curves), resulting from the initial state  $|\rightarrow\rangle^{\otimes L}$ . As a comparison, we also show  $S(t)$  for circuits without conservation law (dashed curves). In all cases, we have  $L = 512$  and periodic boundary conditions.



where  $\alpha' = \alpha/2$  to allow comparison with the random circuits [S4, S8], and we set  $J = 1, h_z = 0.8090, h_x = 0.9045$ . Although the results are limited by small system sizes ( $L = 22$ ), the overall behavior is similar to the Clifford circuits: for  $\alpha = 5$  there is a crossover from  $t$  to  $\sqrt{t}$  growth at long times, while for  $\alpha = 2$  the growth remains  $\propto t$  before saturating, consistent with Eq. (2) in the main text. This suggests that our findings for Clifford circuits can carry over to chaotic many-body quantum systems with long-range interactions. Furthermore, the data in Fig. S9 demonstrates that constrained entanglement growth occurs not only for models with charge conservation (such as in the main text), but applies also more generally for other conservation laws [S6]. In fact, the Ising model in Eq. (S18) does not conserve the total magnetization, but only has total energy as a conserved quantity and exhibits diffusive energy transport in the short-range limit [S7].

### Two-dimensional circuits

Given the efficient simulability of Clifford circuits, we are able to study transport and entanglement growth also in two-dimensional long-range quantum systems, which would otherwise be challenging even for state-of-the-art numerical techniques. We consider circuits with square geometry and total qubit number  $L^2 = L \times L$ . Similar to the 1d case discussed in the main text, a single time step is defined as the application of  $L^2$  random two-qubit gates of range  $r$ , drawn according to the probability distribution  $P(r) \propto r^{-\alpha}$ . Specifically, for two qubits at positions  $(x_1, y_1)$  and  $(x_2, y_2)$ , we define  $r$  as

$$r = |x_1 - x_2| + |y_1 - y_2|. \quad (\text{S19})$$

Analogous to our analysis in Fig. 2, we study transport by considering the U(1)-symmetric Clifford evolution of an isolated  $Z$  operator initially defined at the central site of the  $2d$  lattice,  $\mathcal{U} Z_{\frac{L}{2}, \frac{L}{2}} \mathcal{U}^\dagger$ . Crucially, the picture of long-range random walks of the single  $Z$  operator discussed in the main text generalizes directly to higher-dimensional lattices, i.e., for a single circuit realization the operator will always remain of length one. For the circuit-averaged dynamics of the  $Z$  excitation, the U(1) conservation law then leads to a power-law decay,  $\langle Z_{\frac{L}{2}, \frac{L}{2}}(t) \rangle \propto t^{-d/z}$ , which reflects the different  $\alpha$ -dependent hydrodynamic regimes. In particular, based on the prediction from Lévy flights (see [S5]), we expect diffusion ( $z = 2$ ) for  $\alpha \geq d + 2$ , while  $z = \alpha - d$  for  $d < \alpha \leq d + 2$ , and a breakdown of hydrodynamics for  $\alpha < d$ . For  $d = 2$ , this yields

$$z = \begin{cases} 2, & \alpha \geq 4 \\ \alpha - 2, & 2 < \alpha \leq 4 \end{cases}. \quad (\text{S20})$$

Let us emphasize again that for Hamiltonian systems with coupling constant  $J \propto r^{-\alpha'}$ , these bounds have to be rescaled according to  $\alpha = 2\alpha'$  [S4, S5]. Focusing on  $\alpha = 6, 3.5, 3$ , Fig. S10 (a) unveils a convincing agreement of our numerics with Eq. (S20), where we consider  $\langle Z_{\frac{L}{2}, \frac{L}{2}}(t) \rangle$  in circuits of size  $40 \times 40$ . Note that for smaller  $\alpha$ , the analysis becomes more difficult due to finite-size effects.

We now turn to entanglement dynamics in  $2d$  circuits. To this end, we consider circuits with periodic boundary conditions and calculate  $S(t)$  for a half-system bipartition. In Figs. S10 (b) and (c), we show  $S(t)$  for circuits without

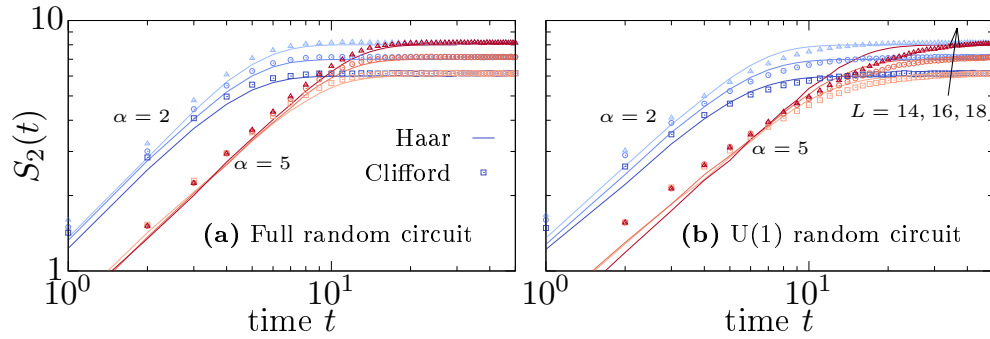


FIG. S8. Entanglement  $S(t)$  for  $\alpha = 2$  and  $\alpha = 5$  in circuits (a) without conservation law and (b) with U(1)-symmetric gates. We compare the case of random Clifford circuits (symbols) to circuits where the two-site gates are randomly drawn according to the Haar measure (curves). Data is shown for circuits with  $L = 14, 16, 18$  and periodic boundaries. While for Clifford circuits all Rényi entropies are equivalent, we show  $S_2(t)$  for Haar-random circuits.

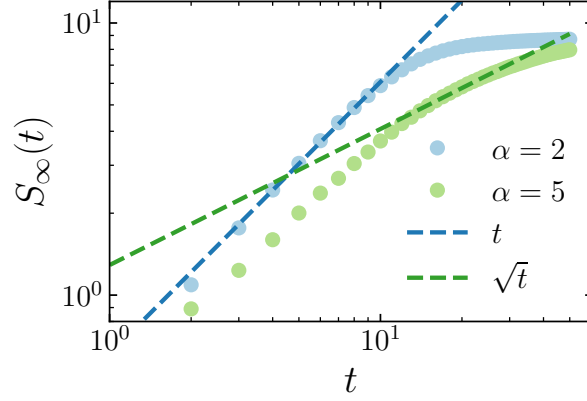


FIG. S9.  $S_\infty(t)$  for different  $\alpha$  in the long-range tilted field Ising model with  $L = 22$ , showing similar behavior to the Clifford circuits. The results are averaged over initial product states, but sample-to-sample fluctuations are small.

conservation law as well as for U(1)-symmetric Clifford circuits, where we again focus on  $\alpha = 6, 3.5, 3$ . As expected, the growth of  $S(t)$  is notably slower in U(1)-symmetric circuits due to the constraint imposed by the conservation law. However, as was already discussed in Ref. [S9], we find that it is actually rather difficult to observe the conjectured asymptotic scaling  $S(t) \propto t^{1/z}$ . Therefore, we here proceed analogous to our analysis in the context of Fig. 4 and extract the saturation time  $t_{\text{sat}}$  of  $S(t)$  for circuit sizes ranging from  $50 \times 50$  to  $90 \times 90$ , see Figs. S10 (d) and (e). [See labels next to the data in Figs. S10 (d) and (e) for the obtained values of  $z$ .] In particular, for circuits without conservation law and  $\alpha = 6$ , we recover the expected linear growth of  $S(t)$  with  $z \approx 1$ . In contrast, for U(1)-symmetric circuits, we find a substantially larger value  $z \approx 1.79$ , which is however smaller than the conjectured value  $z = 2$ . The deviation from the diffusive value may be due to finite-size effects [S9], and we note that similar deviations also occurred in  $1d$  circuits discussed in Fig. 4. Interestingly, for  $\alpha = 3$ , we find that the scaling of  $t_{\text{sat}}$  becomes again rather similar for both circuit variants. Analogous to our discussion of  $1d$  circuits in the main text, this finding can be understood due to the fact that transport becomes sufficiently fast for  $\alpha \leq 3$  in  $2d$ , such that the presence of the hydrodynamic mode becomes less and less relevant.

- 
- [S1] A. D. Córcoles, J. M. Gambetta, J. M. Chow, J. A. Smolin, M. Ware, J. D. Strand, B. L. T. Plourde, and M. Steffen, Phys. Rev. A **87**, 030301(R) (2013).  
[S2] R. Koenig and J. A. Smolin, J. Math. Phys. **55**, 122202 (2014).  
[S3] V. Khemani, A. Vishwanath, and D. A. Huse, Phys. Rev. X **8**, 031057 (2018).

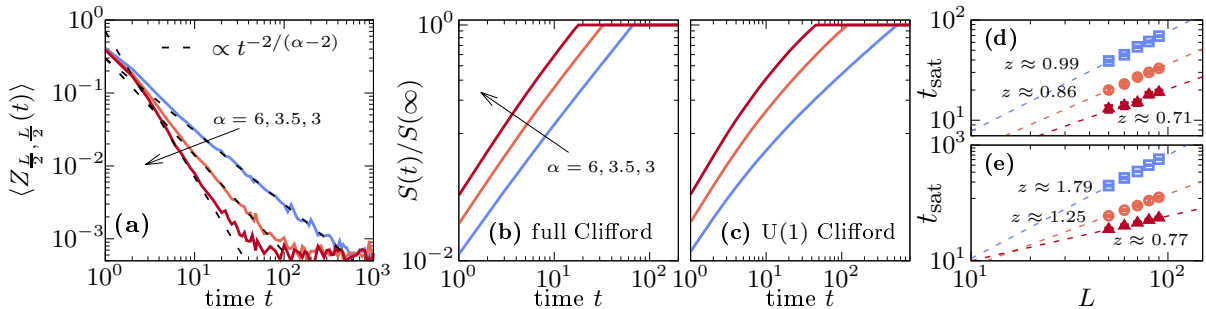


FIG. S10. Transport and entanglement growth in  $2d$  lattices. (a)  $\langle Z_{\frac{L}{2}, \frac{L}{2}}(t) \rangle$  for different  $\alpha$  and  $L = 40$ . Dashed lines indicate power-laws  $\propto t^{-d/(\alpha-d)}$ . (b)  $S(t)$  for a half system bipartition under full Clifford evolution with  $\alpha = 6, 3.5, 3$  in  $90 \times 90$  lattice with periodic boundaries. (c) Analogous to (b), but now for Clifford circuits with U(1) conservation law. [(d), (e)] Saturation time  $t_{\text{sat}}$  of  $S(t)$  versus  $L \in [50, 90]$  for full and U(1)-symmetric circuits. The exponent  $z$  of the fitted power-law scaling  $t_{\text{sat}} \propto L^z$  is indicated next to the data. For  $\alpha \lesssim 3$ , the scaling in circuits with and without conservation law is found to become similar.

- [S4] T. Zhou, S. Xu, X. Chen, A. Guo, and B. Swingle, Phys. Rev. Lett. **124**, 180601 (2020).
- [S5] A. Schuckert, I. Lovas, and M. Knap, Phys. Rev. B **101**, 020416 (2020).
- [S6] T. Rakovszky, F. Pollmann, and C. W. von Keyserlingk, Phys. Rev. Lett. **122**, 250602 (2019).
- [S7] H. Kim and D. A. Huse, Phys. Rev. Lett. **111**, 127205 (2013).
- [S8] M. Block, Y. Bao, S. Choi, E. Altman, and N. Y. Yao, Phys. Rev. Lett. **128**, 010604 (2022).
- [S9] M. Žnidarič, Commun. Phys. **3**, 100 (2020).